ANNALS OF GEOPHYSICS, 67, 5, GC545, 2024; doi:10.4401/ag-9013
OPEN ACCESS

Physics of the Northern Annular Mode – Part 1: connection to meridional mass transfer

Aarnout J. van Delden[*,1]

(1) Institute for Marine and Atmospheric Research Utrecht (IMAU), Physics Department Utrecht University, Utrecht, the Netherlands

Article history: received September 28, 2023; accepted April 09, 2024

Abstract

The Northern Annular Mode (NAM) of atmospheric variability is manifested and identified foremost as coupled variability of (1) the latitude of the most intense zonal-mean surface westerlies in the Northern Hemisphere, (2) the intensity of the zonal-mean subtropical jet (STJ) in the Northern Hemisphere and (3) the difference in zonal-mean sea-level pressure between high pressure in the subtropics (≈35°N) and low pressure at subpolar latitudes (≈65°N). The extreme phases of the NAM are referred to as the positive NAM-phase (weak STJ, very poleward position of the maximum surface westerlies and large meridional sea-level pressure gradient) and the negative NAM-phase (intense STJ, very equatorward position of the maximum surface westerlies and weak or sometimes reversed meridional sea-level pressure gradient).
Because the zonal-mean state of the atmosphere is in close thermal wind balance, zonal-mean mass- and vorticity-distributions are connected by the presence of a positive potential vorticity (PV) anomaly, which defines the lowermost stratosphere and induces the STJ and its associated tropospheric baroclinicity. The amplitude of this PV-anomaly is reduced at high (low) latitudes due to poleward (equatorward) isentropic baroclinic eddy-driven shifts of mass during the negative (positive) NAM-phase. This sharpens (weakens) the meridional gradient of PV in the subtropics. Adjustment to zonal-mean thermal wind balance intensifies (weakens) tropospheric baroclinicity below the PV-anomaly and intensifies (weakens) the STJ during the negative (positive) NAM-phase. A feedback loop is identified, which explains the persistence of the negative NAM-phase. This loop features the zonal-mean baroclinicity at the edge of the subtropics and zonal-mean isentropic eddy-driven mass flux divergence in the lowermost stratosphere just poleward of the subtropics.

Keywords: Subtropical Jet; Meridional Mass Circulation; Balance; Baroclinic; Lowermost Stratosphere

1. Introduction

This research paper is part one of two papers aiming to describe and explain the seasonal and non-seasonal variability of the eastward (= westerly) winds in the middle latitudes of the Northern Hemisphere, in relation to the zonal-mean distribution of mass and vorticity in the atmosphere. Using re-analysis data, coupled physical processes are identified that might explain the remarkable persistence, over periods of weeks, of either abnormally

weak or abnormally intense zonal-mean eastward winds in the Northern Hemisphere winter, both at the earth's surface and in the upper troposphere (Baldwin et al., 2003). These periods represent the two phases of a mode of atmospheric variability, known as the "Zonal Index Cycle" (Namias, 1950) or "Northern Annular Mode" (NAM) (Li and Wang, 2003).

At the earth's surface, the negative (positive) phase of the NAM is manifest as lower (higher) than average zonal-mean sea-level pressure in the subtropics (latitude, $\phi \approx 35°$N) together with higher (lower) than average zonal-mean sea-level pressure in the subpolar regions ($\phi \approx 65°$N). It is shown here that this reflects the variability of the eddy-driven exchange of mass between the subtropics and the subpolar latitudes.

Long term average, zonal-mean "surface-westerlies", which by convention are measured at 10 meters above the earth's surface, are most intense at a latitude of approximately 40°N in winter and at about 50°N in summer (Fig. 1a). The intensity of the westerlies in the atmosphere increases with height, culminating in the Sub-Tropical Jet (STJ) at a pressure, p approximately equal to 200 hPa, corresponding approximately to a potential temperature,

$$\theta = T\left(\frac{p_{ref}}{p}\right)^{\kappa} = 350\ \mathrm{K}. \tag{1}$$

Here, T is temperature, p_{ref} is a constant reference pressure (= 1000 hPa) and $\kappa = R/c_p$, where R is the specific gas constant of air and c_p is the specific heat of air at constant pressure. The STJ in the Northern Hemisphere is observed at or very near to the isentropic level (constant θ-level) corresponding to $\theta = 350$ K. The latitude of the STJ and the intensity of the STJ, however, exhibit a significant seasonal cycle (Fig. 1b). In winter and in early spring an intense STJ is observed at about 30°N, while in summer and early autumn a much weaker STJ is observed as far poleward as 45°N.

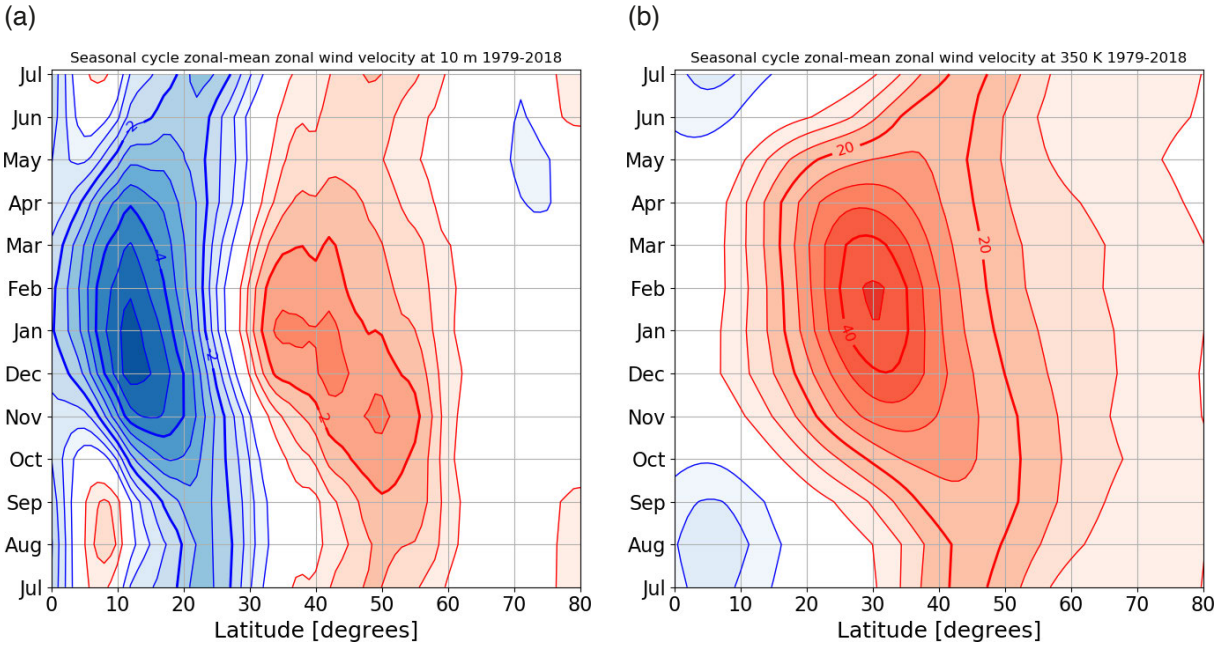

Figure 1. Seasonal cycles of the zonal-mean wind velocity near the surface (a) and at $\theta = 350$ K (about 200 hPa) (b). (a) Ensemble (1979-2018) monthly mean zonal-mean surface westerly wind velocity as a function of month and latitude in the Northern Hemisphere. Contours drawn every 0.5 m/s (0 m/s – contour is not drawn). Blue shading: $[u] \leq 0.5$ m/s (surface-easterlies); red shading: $[u] \geq 0.5$ m/s (surface-westerlies). (b) Ensemble (1979-2018) monthly mean zonal-mean zonal velocity at $\theta = 350$ K as a function of month and latitude in the Northern Hemisphere. Contours are drawn every 5 m/s (0 m/s – contour is not drawn). Red shading indicates westerly winds. The sub-tropical jet (STJ) is located approximately at $\theta = 350$ K. The equatorward shift of the surface westerlies and simultaneous intensification of the STJ between November and February is placed into the context of the theme of this paper in section 7. Based on the monthly mean ERA-Interim reanalysis (Dee et al., 2011).

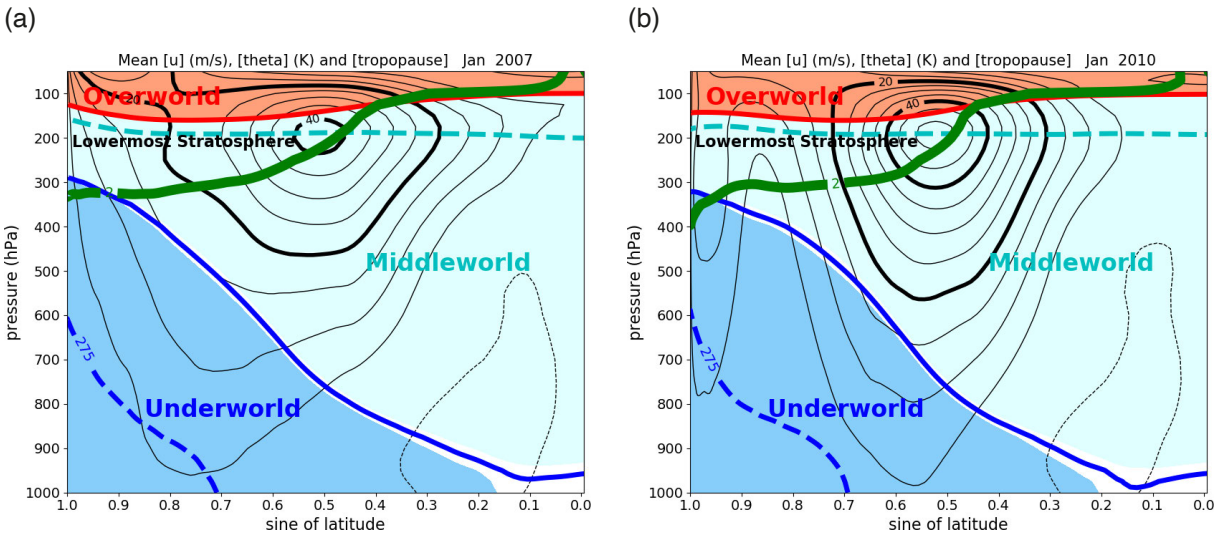

Figure 2. The schematic division of the zonal-mean atmosphere into the Underworld (blue shading), the Middleworld (cyan shading) and the Overworld (red shading) (explained in detail in section 2). Monthly mean zonal-mean zonal wind velocity (solid and dashed black lines, labeled in m/s, interval: 5 m/s; zero contour not drawn, dashed contours correspond to easterly winds) as a function of pressure and the sine of latitude, for January 2007 ((a); positive NAM phase) and for January 2010 ((b); negative NAM phase). The green solid line is the 2 PVU isopleth of zonal-mean potential vorticity, defined as the zonal mean dynamical tropopause. Selected isentropes are shown in solid blue ($\theta = 300$ K), dashed cyan ($\theta = 350$ K) and solid red ($\theta = 370$ K). The Underworld appears as a dome of cold air, centered over the North Pole. The lowermost stratosphere is defined as that part of the Middleworld, which lies in the stratosphere. Based on monthly mean ERA-Interim reanalysis (Dee et al., 2011).

On time-scales of weeks to months the westerlies may deviate appreciably from the long-term average seasonal cycle, shown in Fig. 1.

Figure 2 shows cross sections of the time-mean zonal-mean state of the atmosphere in January 2007 (a) and in January 2010 (b). January 2007 is representative for the extreme positive NAM-phase, while January 2010 is representative for the extreme negative NAM-phase. In both months the STJ-core is observed at 30°N and $\theta = 350$ K ($p = 200$ hPa), but the STJ is much more intense in 2010 than in 2007, while the maximum surface-westerlies are observed much farther poleward in 2007 than in 2010.

The division of the atmosphere into Underworld, Middleworld and Overworld (Fig. 2), following Hoskins (1991), is explained in section 2.

The extreme phases of the NAM frequently persist for a week or much longer, and may bring recurring extreme weather, such as cold spells in winter in Central Europe and Central Asia together with above average precipitation in winter in Southern Europe and Northern Africa during the negative NAM-phase, as in January 2010 (Cattiaux et al., 2010; Riviere and Drouard, 2015), or very stormy, wet and mild winter weather in Central Europe together with very dry conditions in Southern Europe and Northern Africa during the positive NAM-phase, as in January 2007 (Fink et al., 2009).

The NAM is also known as the Arctic Oscillation (AO) (Thompson and Wallace, 2000). The AO is defined as the leading Empirical Orthogonal Function of the geopotential height in the troposphere of the Northern Hemisphere (Thompson and Wallace, 1998). The North Atlantic regional manifestation of the NAM, or AO, is known as the North Atlantic Oscillation (NAO), which in its most simple formulation is defined as the sea-level pressure difference between Reykjavik and Lisbon (Hurrell, 1995). The North Pacific regional manifestation of the NAM, or AO, is the North Pacific Oscillation (NPO) (Rogers, 1981). Here, the NAM is identified, by definition, with non-seasonal component of fluctuations in the zonal-mean state of the extra-tropical atmosphere. In contrast to this definition, the AO, NAO and NPO are obviously not zonally symmetric.

A physical interpretation of the NAM is based on the idea that the dynamical structure of the atmosphere can be divided into the following three interacting components. (1) a "primary" zonally symmetric (zonal-mean) circumpolar circulation, (2) a "secondary" zonally symmetric *meridional* circulation (the Hadley- and Ferrel cells), and (3) eddies and waves, or zonal asymmetries. The NAM is identified with the intensity and structure of the

zonally symmetric primary circulation. We will see that the primary circulation is in very close thermal wind balance, which means that it is associated with a specific distribution of mass and vorticity. A theory of the NAM must identify positive feedbacks in the physical interactions between the three components of the atmospheric circulation, which can maintain the NAM in an extreme phase for an appreciable time. These physical interactions express themselves as couplings between isentropic meridional fluxes of mass and vorticity due to, respectively, the secondary circulation (component 2) and eddies (component 3), which lead to shifts in the intensity and structure of the primary circulation and its associated distribution of mass and vorticity.

Lorenz (1951) associated the Zonal Index Cycle in the Northern Hemisphere with shifts of atmospheric mass between the Polar regions and the subtropics. Much later, Baldwin (2001) stated that NAO, NPO, AO and NAM are imprints of the movement of atmospheric mass between the Polar cap and the region equatorward of 55°N. In view of these early insights, it is surprising that the link between NAO, NPO, AO or NAM and the meridional circulation of mass has never received any explicit attention in the scientific literature. Probably, this is because mass fluxes do not appear in the mass conservation equation when pressure (p) is used as a vertical coordinate, which is by far the preferred vertical coordinate in the atmospheric science community. This paper takes a different approach by adopting potential temperature (θ) as a vertical coordinate, following Johnson (1989). In the θ-coordinate system, the general circulation of the atmosphere is analyzed in terms of vorticity and isentropic density, or mass. Vorticity and isentropic mass-density determine potential vorticity, a variable which is central in large scale atmospheric dynamics, as we shall see in section 5.

Because of its zonal symmetry, the NAM, as defined here, is relatively easily connected to a physics-based mathematical theory, which describes and predicts the zonal-mean mass- and vorticity-distributions and the associated zonal-mean circumpolar flow, in relation to meridional fluxes of mass and vorticity due to eddies and due to the secondary circulation. AO, NAO and NPO are purely statistical quantities, which cannot be identified with a variable in any physics-based equation.

This research paper (part 1) shows that the NAM is maintained in its negative phase by intense eddy-driven poleward mass fluxes in a feedback loop with baroclinicity, while a follow-up research paper (part 2) (van Delden, 2024) demonstrates that intense eddy-driven meridional vorticity fluxes are crucial in maintaining the NAM in its positive phase.

Sections 2-6 of part 1 describe the zonal mean structure of the atmosphere in isentropic coordinates, regarding in particular the intimately connected zonal-mean distributions of mass (or isentropic density) and isentropic vorticity. Section 2 describes the gross properties of the structure of the zonal-mean state of the atmosphere, specifically its division into three layers bounded by either the earth's surface and suitably selected isentropic surfaces, and the relation of these layers to the tropopause and the so-called "lowermost stratosphere". Section 3 introduces the mass conservation equation in isentropic coordinates and defines the zonal-mean meridional isentropic mass flux, divided into contributions due to, respectively, the secondary circulation and eddies. The stationary zonal-mean circulation of mass, derived from the net isentropic mass flux, is introduced. Section 4 demonstrates that the primary circumpolar circulation is in a state very close to thermal wind balance. This implies that the westerly wind and its associated vorticity distribution is linked to the distribution of mass. The physical nature of this link can be understood from the solution of the zonal-mean "potential vorticity (PV) inversion equation", as is demonstrated in section 5. Again, this is seen and understood best in isentropic ($\theta-$) coordinates. Several robust relations between the zonal-mean Northern Hemispheric isentropic distributions of PV, vorticity and density are revealed by the solution of the PV-inversion equation. PV-inversion reveals that the latitude and intensity of the STJ in a zonally symmetric atmosphere in thermal wind balance are linked to a sharp meridional PV-gradient in the Middleworld. Section 6 is concerned with identifying physical processes and mechanisms that explain the sharp meridional PV-gradient in the Middleworld.

The second part of this research paper (sections 7 and 8) examines how the NAM is manifest at the earth's surface in terms of sea-level pressure and proceeds to show that these manifestations are strongly linked to the zonal-mean meridional mass flux in the extra-tropics. After addressing some synoptic aspects of the seasonal cycle of the distribution of sea-level pressure in the Northern Hemisphere in section 7, section 8 proceeds to define a measure for the strength of the NAM at the earth's surface (a so-called NAM-index), based on zonal mean sea-level pressure, and demonstrates that the negative NAM-phase is associated with a more intense and deeper than average circulation of mass. A positive feedback-loop is identified between the intensity of the upper poleward branch of the mass flux circulation and STJ-intensity, which maintains the NAM in its extreme negative phase. The paper is concluded in section 9 with a list of physical processes that might break this positive feedback-loop and so usher in a feedback loop which maintains the positive NAM-phase.

2. The Polar Cold Air Dome, or Underworld

A large part of the atmospheric mass in the Northern Hemisphere is trapped in a "cold air dome" over the snow- and ice-covered surface (Nagle, 1979; Johnson, 1989). In the zonal-mean portrayal of the thermal structure of the atmosphere, shown in Fig. 2, this cold air dome, defined as the air mass below $\theta = 300$ K, is centred over the North Pole. Following the terminology introduced by Shaw (1913), the cold air dome is referred to as the "Underworld". Hoskins (1991) defined the Underworld as consisting of all isentropic surfaces, which intersect the earth's surface. The upper limit of the Underworld in January is $\theta = 300$ K. Air can enter the Underworld only by radiative cooling and escape by radiative heating and latent heat release.

The layer directly above the Underworld is called "Middleworld". According to Hoskins (1991), the defining characteristic of the Middleworld is that it intersects the dynamical tropopause. The dynamical tropopause is defined as the isopleth of potential vorticity corresponding to 2 "Potential Vorticity Units" (PVU) ($1\ \mathrm{PVU} = 10^{-6}\ \mathrm{m^2 K\, s^{-1} kg^{-1}}$). In isentropic coordinates, potential vorticity (Z) is defined as absolute vorticity (ζ_a) divided by isentropic density (σ), i.e.

$$Z = \frac{\zeta_a}{\sigma}, \tag{2}$$

where isentropic density (σ) is defined as

$$\sigma = -\frac{1}{g}\frac{\partial p}{\partial \theta} \tag{3}$$

(g represents the acceleration due to gravity). Potential vorticity (PV) is conserved in adiabatic (isentropic) circumstances.

The upper boundary of the Middleworld, or lower boundary of the overlying layer, called "Overworld", coincides with the isentropic level which intersects the tropical "cold point tropopause", identified with the tropical temperature minimum at $p \approx 100$ hPa or $\theta \approx 370$ K.

The definition of the Middleworld by Hoskins (1991) does not hold for the warm months from May to September in the Northern Hemisphere. The lower part of Middleworld in these months lies entirely in the troposphere. Therefore, the most accurate and simple general definition of the Middleworld is that this layer consists of all isentropes that do not fit the definition of the Underworld and the Overworld.

The stratospheric part of the Middleworld is called "lowermost stratosphere" (Dessler et al., 1995; Holton et al., 1995; Appenzeller et al., 1996). This part of the extra-tropical Middleworld is characterized by low isentropic density relative to the isentropic density at the same isentropic level in the troposphere (i.e. in the tropics). In January, the lowermost stratosphere is identified almost completely with the extra-tropical Middleworld. The STJ, both in January and July, is observed at the boundary between the tropical and extra-tropical Middleworld (Fig. 2). This boundary, also identified as the isentropic tropopause (Ambaum, 1997), is characterized by an abrupt change in the isentropic density from high isentropic density in the tropics to low isentropic density at higher latitudes. Section 5 shows that the relative low isentropic density of the extra-tropical Middleworld is due to cross-isentropic mass flux divergence at high latitudes, which feeds the Underworld. Section 5 also shows that the STJ-intensity depends on the isentropic density gradient at the boundary between the extra-tropical Middleworld and the tropical Middleworld.

3. The stationary residual mean meridional circulation of mass

The standard textbook view (Holton, 2004, p. 327) of the zonal-mean circulation of mass assumes stationary conditions. Stationary conditions imply putting local time-derivatives equal to zero, which translates into zero zonal-mean mass flux divergence, i.e.

$$\frac{\partial}{a\partial\phi}\left([v\sigma]\cos\phi\right) + \cos\phi\frac{\partial}{\partial\theta}\left(\left[\frac{d\theta}{dt}\sigma\right]\right) = 0. \tag{4}$$

Here, u and v, are, respectively, the zonal (x) and meridional (y) components of the velocity, ϕ is latitude, square brackets indicate a zonal-mean and a is the radius of the earth, assumed constant ($a = 6371$ km). Zero total mass flux divergence is a reasonable assumption for an average year or maybe for an ensemble-average of many January-months (Fig. 8a of Johnson, 1989; Fig. 1 of Held and Schneider (1999), or Fig. 5.3 of Randel, 2015) or of many sets of consecutive DJF-months (Fig. 2 of Cai and Shin, 2014).

The mass flux streamfunction, Ψ, which satisfies Eq. (4), is defined as,

$$2\pi a[v\sigma]\cos\phi \equiv \frac{\partial\Psi}{\partial\theta}; \quad 2\pi a\left[\frac{d\theta}{dt}\sigma\right]\cos\phi \equiv \frac{\partial\Psi}{\partial y}. \tag{5}$$

Here $y = a\phi$. The factor $2\pi a$ is inserted in Eq. (5) so that Ψ has the same unit (kg s^{-1}) and physical meaning as the "velocity" stream function, which is used to portray the Hadley circulation and the Ferrel circulation (Randel, 2015).

We use ERA-Interim reanalysis data (Dee et al., 2011)[1] of the meridional velocity, v, and pressure, p, on isentropic surfaces to evaluate the time-mean (indicated by an overbar) zonal-mean (indicated by square brackets) meridional isentropic mass flux, defined as

$$\overline{[v\sigma]} = \frac{1}{\tau}\int_0^\tau [v\sigma]\,dt, \tag{6}$$

where $\tau = 40 \times 31$ days, corresponding to all 40 months of January in the years, 1979-2018. The time integral in Eq. (6) is evaluated in steps of 6 hours. The pressure is given at 14 isentropic levels corresponding to 265 K, 275 K, 285 K, 300 K, 315 K, 330 K, 350 K, 370 K, 395 K, 430 K, 475 K, 530 K, 600 K and 700 K. Isentropic density for layers between these isentropic levels is evaluated from the pressure difference between these isentropic levels. The meridional mass flux in a particular layer is evaluated at 6-hour intervals using the average of v at the upper and lower boundary of the layer. The cross-isentropic mass flux at the highest isentropic level of the re-analysis data used here ($\theta = 700$ K) is assumed to be negligibly small because σ at this level is very small also. Therefore, the boundary condition, $\Psi = 0$ at $\theta = 700$ K is imposed. Numerical integration of the time-mean of the first equation in (5), i.e. by applying

$$\frac{\partial\overline{\Psi}}{\partial\theta} = 2\pi a\,\overline{[v\sigma]}\cos\phi \tag{7}$$

from the top of the domain downward, yields $\overline{\Psi}$ as a function of ϕ and θ. The vertical integration stops when the isentropic level is below the earth's surface. This requires information about the potential temperature at the earth's surface.

The result of this exercise, i.e. the January ensemble-mean stationary meridional circulation of mass for the years 1979-2018, is shown in Fig. 3. We observe two loosely connected circulation cells in each hemisphere. In both the tropical cell and the mid-latitude cell, air moves poleward at high isentropic levels and equatorward at low isentropic levels. The cross-equatorial tropical cell, known as the winter Hadley cell, is driven principally by latent heat release in the updraft of this circulation between the equator and 15°S, while the mid-latitude cell is driven principally by isentropic mass- and vorticity fluxes due to eddies.

To evaluate the contribution of eddies to the isentropic mass flux, we start by writing v and σ as a sum of the zonal-mean, indicated by square brackets, and a perturbation with respect to the zonal mean, indicated by an asterisk, as

$$v \equiv [v] + v^*; \quad \sigma \equiv [\sigma] + \sigma^*. \tag{8}$$

1 The fourth generation ECMWF atmospheric reanalysis of the global climate, called "ERA-Interim", was the best reanalysis available from ECMWF in the year 2017, when this research project was initiated. An updated fifth generation reanalysis for the same period, called "ERA5", is now available from ECMWF. The author is convinced that the results described in this paper and the companion paper will not or hardly be affected by changes produced by the ERA5 reanalysis to the ERA-Interim reanalysis for the years in question (1979-2018).

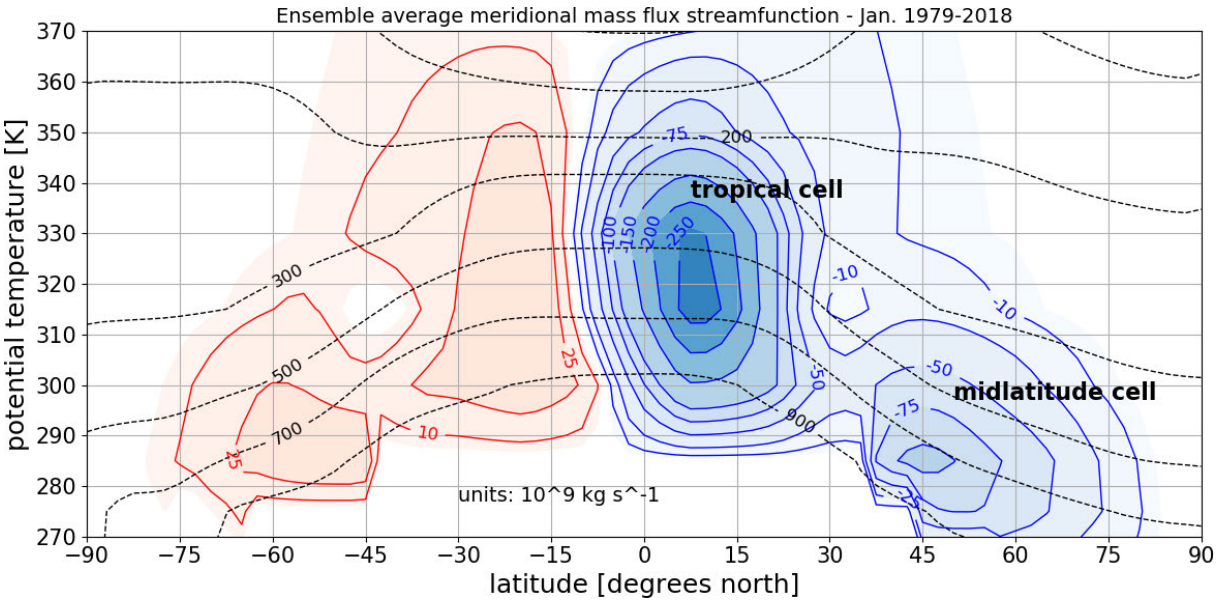

Figure 3. January ensemble-mean, for the years 1979-2018, stationary residual circulation of mass. Solid contours, labeled in units of 10^9 kg s^{-1}, are isopleths of mass flux streamfunction, $\overline{\Psi}$, while dashed contours, labeled in hPa, are isopleths of pressure. Blue shading: clockwise circulation. Red shading: anti-clockwise circulation. Based on the 6 hourly ERA-Interim reanalysis (Dee et al., 2011).

The net zonal-mean isentropic meridional mass flux can be expressed as follows.

$$[v\sigma] = \left[[v][\sigma] + [v]\sigma^* + [\sigma]v^* + v^*\sigma^*\right] = [v][\sigma] + v^*\sigma^*. \tag{9}$$

The first term on the right hand side of Eq. (9) represents the meridional mass flux due to the secondary circulation while the second term represents the meridional mass flux due to eddies. It is stressed that Eq. (9) is exact and not the result of linearization. Figure 4 shows the time-evolution of the net zonal-mean isentropic meridional mass flux at 50°N in the layer between $\theta = 300$ K and $\theta = 330$ K, and the contributions of eddies and the secondary circulation to this mass flux, as a function of time in both January 2007 and January 2010. The contribution of eddies is mostly positive (poleward), while the contribution of the secondary circulation, which is also called the "Ferrel cell", is mostly negative (equatorward).

The eddy mass flux is frequently countered by the mass flux due to the secondary circulation, especially in January 2007. Because of this, the net zonal-mean isentropic meridional mass flux is referred to as the "residual mass flux". The stationary circulation shown in Fig. 3 is known as the "residual mean meridional circulation" (Rosenlof, 1995). Its stratospheric manifestation is known as the "Brewer-Dobson circulation" (Butchart, 2014).

At 50°N and 315 K, the mass flux due to the secondary circulation counters the eddy mass flux quite systematically much more in January 2007 than in January 2010. This is an important reason why the net (residual) mostly poleward mass flux is in general relatively weak in January 2007, as explained in more detail in part 2 of this research paper (van Delden, 2024).

The poleward net isentropic mass flux in the mid-latitudes above 290 K in January 2007 (Fig. 4a) is determined by short bursts, lasting 1-4 days, in the first part of the month, and by two relatively intense bursts of poleward mass flux lasting 6 and 4 days, respectively, in the latter part of the month. The poleward net isentropic mass flux in the mid-latitudes above 290 K in January 2010 (Fig. 4b) is determined by two intense relatively long-lasting bursts.

4. Balance and baroclinicity

This section demonstrates that the zonal-mean state is in very close balance, both in hydrostatic balance and in gradient wind balance. An equation for gradient wind balance is derived from the y-component of the equation

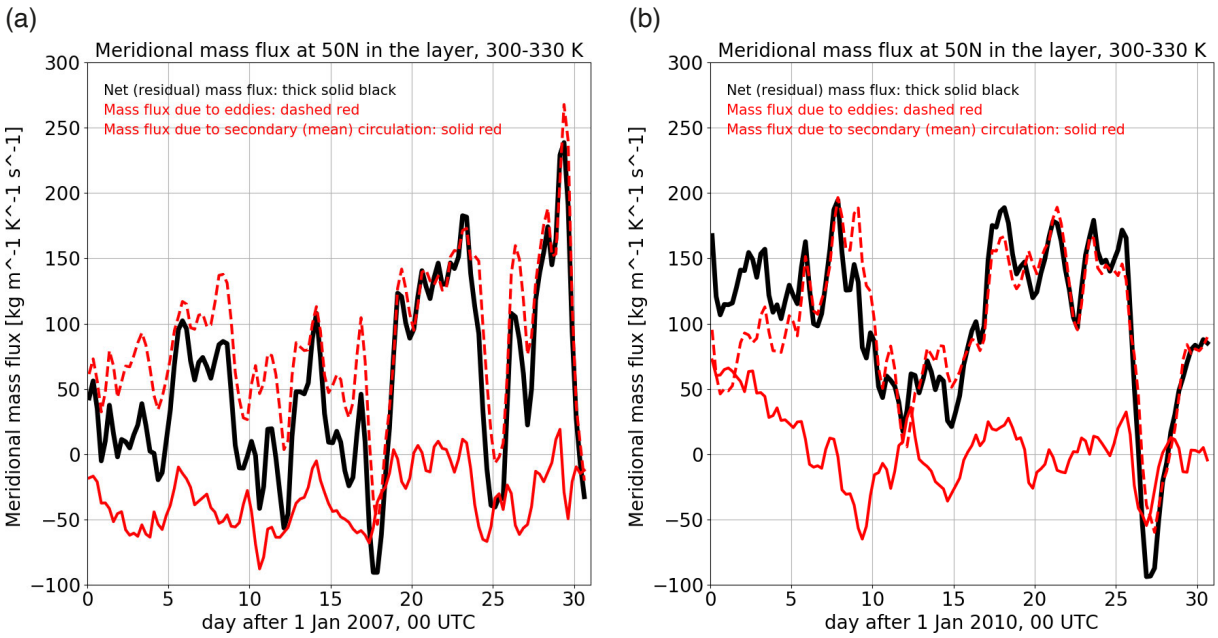

Figure 4. Zonal-mean isentropic meridional mass flux at 50°N in the layer between $\theta = 300$ K and $\theta = 330$ K in units of kg $s^{-1}m^{-1}K^{-1}$, as a function of time in January 2007 (a) and January 2010 (b). Positive is northward. The black solid curve represents the net zonal-mean isentropic meridional mass flux ($[v\sigma]$); the solid red curve represents the zonal-mean isentropic meridional mass flux due to the secondary circulation ($[v][\sigma]$); the dashed red curve represents the zonal-mean isentropic meridional mass flux due to eddies ($[v^*\sigma^*]$). Based on the 6 hourly ERA-Interim reanalysis (Dee et al., 2011).

of motion, assuming that air is not accelerated in meridional (y)-direction. In the isentropic coordinate system (Holton 2004, p. 109) this equation is

$$\frac{tan\,\phi}{a}u_{gr}^2 + f u_{gr} + \left(\frac{\partial \Psi}{\partial y}\right)_\theta = 0. \tag{10}$$

In Eq. (10), u_{gr} is the "gradient zonal wind velocity", $f = 2\Omega \sin\phi$ is the planetary vorticity (or "Coriolis parameter"), with Ω earth's angular velocity, and Ψ is henceforth the isentropic stream function (this symbol was also used for the mass flux stream function in section 3). The isentropic stream function,

$$\Psi \equiv c_p T + g z_\theta. \tag{11}$$

Here, z_θ is the physical height of the isentropic surface above sea level. The other variables are defined in previous sections.

The first (non-linear) term in Eq. (10) is a centrifugal-like acceleration. This term becomes important at high latitudes. The solution of Eq. (10) is

$$u_{gr} = -\frac{b}{2} \pm \frac{b}{2}\sqrt{1 + \frac{4}{b}u_g}, \tag{12}$$

where $b = fa/(cos\phi)$ and the geostrophic wind velocity

$$u_g \equiv -\frac{1}{f}\left(\frac{\partial \Psi}{\partial y}\right)_\theta. \tag{13}$$

Geostrophic winds at individual grid points are determined from Eq. (13) with gridded reanalysis data of the isentropic stream function, after which the balanced gradient wind is determined from Eq. (12) (with the plus sign in front of the second term on the right-hand side). Figure 5 shows instantaneous values, every 6 hours, of the zonal component of the *zonal-mean* gradient wind at two points in the lowermost stratosphere (the extra-tropical Middleworld), plotted against the corresponding actual zonal-mean zonal wind, $[u]$ (horizontal axis). The two points in the lowermost stratosphere are located at $\phi = 50°\text{N}$ and $\theta = 315$ K (a) and at $\phi = 30°\text{N}$ and $\theta = 350$ K (b). Both points are located very close to the dynamical tropopause. Red dots in Fig. 5 correspond to January 2007, while blue dots correspond to January 2010.

Note first that the instantaneous zonal-mean zonal wind, $[u]$, does not deviate very much from the instantaneous balanced wind. Note furthermore that the zonal-mean zonal wind velocity near the core of the STJ, at 30°N and 350 K (Fig. 5b), is systematically stronger in January 2010 than in January 2007, while, roughly speaking, the reverse is the case further north and lower, at 50°N and 315 K (Fig. 5a). A systematic bias towards slightly "super-gradient" zonal-mean zonal winds ($[u] > [u_{gr}]$), exists especially near the STJ-core at 350 K. At higher latitudes zonal-mean zonal winds are systematically super-gradient only if they exceed 20 m s^{-1}. This occurs by far most often in January 2007.

Super-gradient winds may arise either due to conservation of angular momentum when the zonal-mean *meridional* wind velocity, $[v]$, is poleward ($[v] > 0$ in the Northern Hemisphere) or due the action of eddies, which may accelerate the zonal-mean eastward flow because they carry vorticity poleward, as is shown in part 2 of this paper (van Delden, 2024).

The zonal-mean gradient wind is related to the distribution of isentropic pressure, through hydrostatic balance as follows. We begin with the *zonal-mean* gradient wind balance equation (Eq. 10):

$$\frac{([u]^2 + [u^*u^*])\,tan\,\phi}{a} + f[u] + \left(\frac{\partial[\Psi]}{\partial y}\right)_\theta = 0. \tag{14}$$

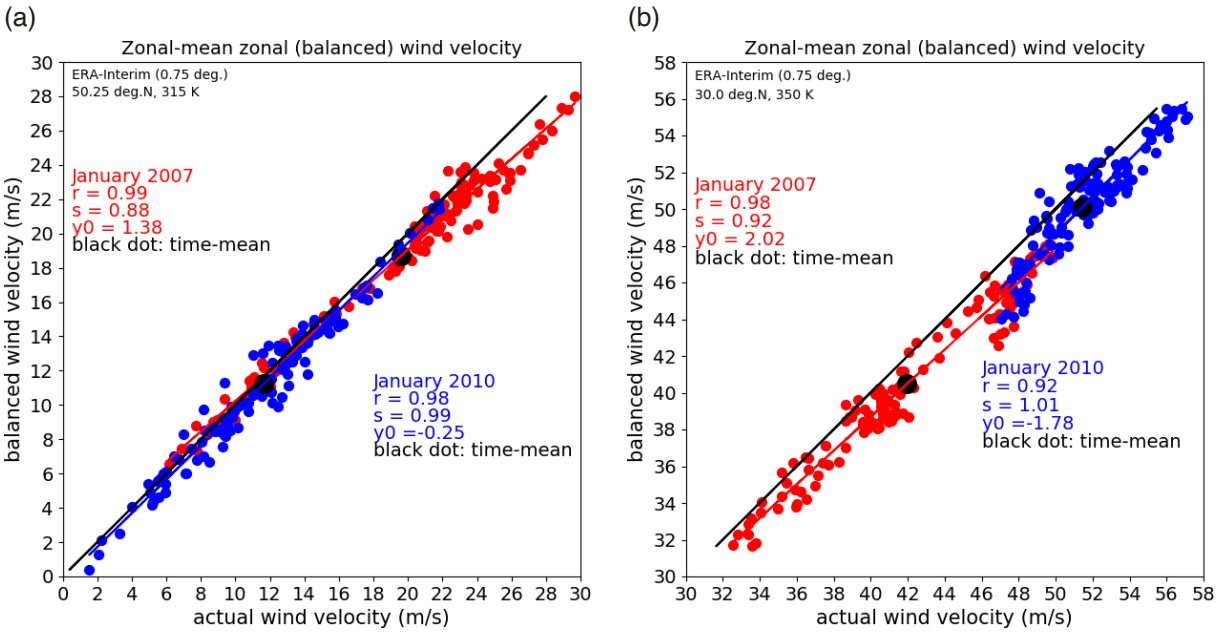

Figure 5. Instantaneous zonal-mean gradient wind velocity ($[u_{gr}]$) (blue: January 2010; red: January 2007) as a function of the instantaneous actual zonal-mean zonal wind velocity ($[u]$), daily at 0, 6, 12 and 18 UTC, at $\theta = 315$ K and 50°N (a) and at $\theta = 350$ K and 30°N (b). Straight red line: best (least squares) linear fit to all points corresponding to January 2007. Straight blue line: best (least squares) linear fit to all points corresponding to January 2010. The slope, s, the correlation coefficient, r, and the value of y_0, at which the best fit intersects the y-axis, are given for each month. The "1 to 1" line is shown in black. The standard error, SEr, of r for all 4 linear fits is less than 0.03. This means that, if we repeat the calculation with a bigger sample (more than 40 years), and if the distribution is "normal" or Gaussian, there is 68% (95%) chance that the correlation coefficient will fall in the range $r \pm$ SEr ($r \pm 2 \times$ SEr) (Rowntree, 1981). Based on 6 hourly ERA-Interim reanalyses (Dee et al., 2011).

If potential temperature increases with increasing height, or with decreasing pressure, the atmosphere is in close hydrostatic balance (van Delden, 2000). For the zonal-mean state this implies that,

$$\frac{\partial[\Psi]}{\partial\theta} = [\Pi], \tag{15}$$

where the Exner function, Π, is defined as

$$\Pi \equiv c_p \left(\frac{p}{p_{ref}}\right)^{\kappa}. \tag{16}$$

Combining Eq. (14) with Eq. (15) and assuming that $[u^*u^*] \ll [u]^2$, yields the thermal wind balance equation:

$$f_{loc}\frac{\partial[u]}{\partial\theta} \equiv -\left(\frac{\partial[\Pi]}{\partial y}\right)_\theta, \tag{17}$$

with

$$f_{loc} \equiv f + \frac{2[u]\,tan\,\phi}{a}. \tag{18}$$

Using the definition of the Exner function (Eq. 16) and the ideal gas law ($p = R\rho T$ where ρ is density and R the specific gas constant of dry air), the right-hand side of Eq. (17) can be rewritten as follows:

$$\left(\frac{\partial[\Pi]}{\partial y}\right)_\theta \approx \frac{1}{\theta[\rho]}\left(\frac{\partial[p]}{\partial y}\right)_\theta, \tag{19}$$

so that thermal wind balance (Eq. 17) becomes

$$f_{loc}\theta[\rho]\frac{\partial[u]}{\partial\theta} \approx -\left(\frac{\partial[p]}{\partial y}\right)_\theta. \tag{20}$$

In a balanced atmosphere, vertical shear of the zonal-mean zonal wind velocity is accompanied by an isentropic meridional pressure gradient (Eq. 20). Figure 6 demonstrates that this is true for the monthly mean zonal-mean state. Regions characterized by a large isentropic meridional pressure gradient are called “baroclinic zones”. The intensity of a baroclinic zone is measured in terms of “baroclinicity”, B, defined as the absolute value of the isentropic pressure gradient. Zonal-mean baroclinicity, $[B]$, is defined as

$$[B] \equiv \left|\left(\frac{\partial[p]}{\partial y}\right)_\theta\right|. \tag{21}$$

In Fig. 6 “baroclinic zones”, defined as regions for which $[B] > 6 \times 10^{-3}$ Pa m^{-1}, are highlighted by red shading. A similar definition of baroclinicity, also called “frontal intensity”, was proposed by van Delden (1999).

The largest values of $[B]$ in the Northern Hemisphere in January are usually encountered close to 30°N and 500 hPa (315 K) (Fig. 6). Significant month-to-month variations exist in the magnitude of $[B]$. $[B]$ is much larger in January 2010 than in January 2007. Consistent with Eq. (20), the STJ in January 2010 is about 10 m s^{-1} faster than the STJ in January 2007.

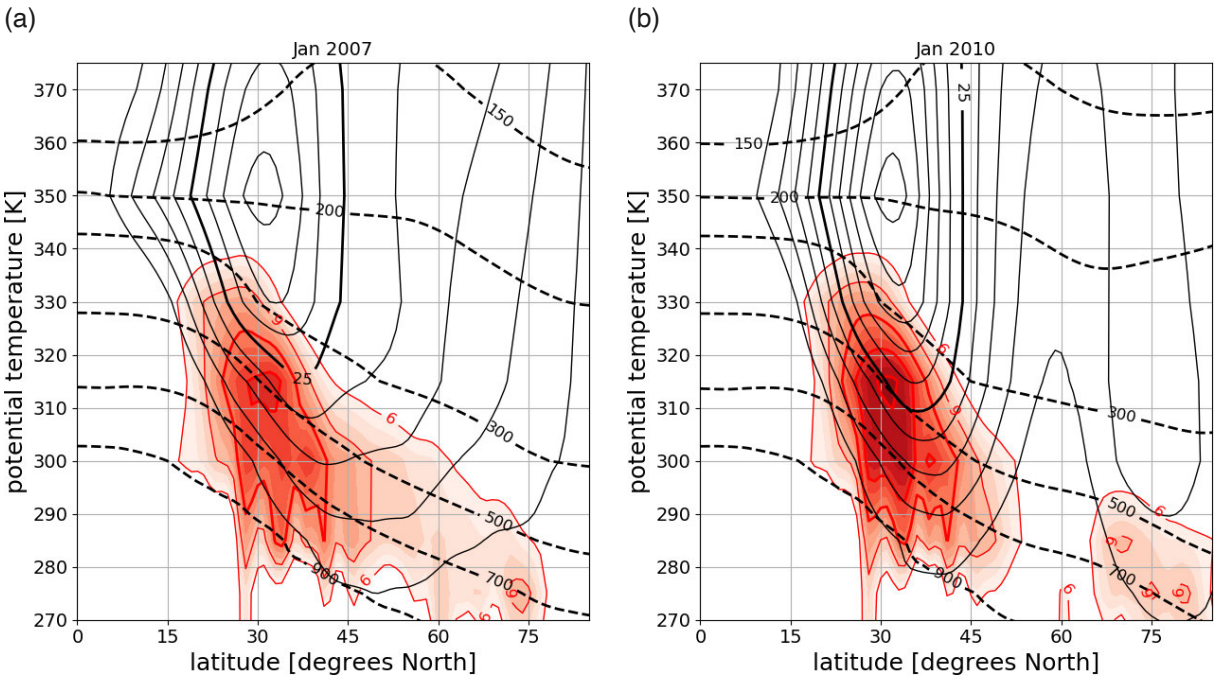

Figure 6. Monthly mean fields of baroclinicity, $[B]$ (Eq. 21) red shading; contour interval is 3×10^{-3} Pa m^{-1}; first contour corresponds to 6×10^{-3} Pa m^{-1}), of $[p]$ (dashed contours, representing 900 hPa, 700 hPa, 500 hPa, 300 hPa, 200 hPa and 150 hPa) and of $[u]$ (solid contours at 5 m/s intervals; zero contour not shown), as a function of potential temperature and latitude, for January 2007 (a) and January 2010 (b). Based on the ERA-Interim reanalysis (Dee et al., 2011).

The time-evolution of $[B]$ is determined by mass flux divergence, first by the divergence of cross-isentropic down- and upwelling, which determines the mean seasonal cycle of the masses in the Underworld and Middleworld, as we shall see in section 5, and second by isentropic meridional mass flux divergence, which, very interestingly, is determined by $[B]$, as we shall see in section 6.

5. The link between vorticity and isentropic density in a balanced atmosphere

This section shows that the primary circulation in an atmosphere in zonal-mean thermal wind balance is determined by zonal-mean potential vorticity (PV) (Eq. 2). Zonal-mean PV in the troposphere and in the lowermost stratosphere is determined principally by planetary vorticity, f, and by zonal-mean isentropic density, especially in the Middleworld. Therefore, it is important to pay attention to the distribution of isentropic density, including its seasonal cycle.

Air masses in, respectively, the Underworld and the Middleworld in the Northern Hemisphere undergo seasonal cycles, which are out of phase (Fig. 7). The Underworld in the Northern Hemisphere contains about 3×10^{17} kg in July and about 7.5×10^{17} kg in January, while the Middleworld, poleward of 30°N, contains about 5×10^{17} kg in July and about 2×10^{17} kg in January. The mass-loss of the extra-tropical Middleworld to the Underworld by cross-isentropic downwelling at $\theta = 300$ K between summer and winter is partly compensated by the mass-gain from the tropics across the sub-tropical jet and from the Overworld across its lower boundary at $\theta = 370$ K. The total mass in the Overworld of the Northern Hemisphere has practically no seasonal cycle because cross-isentropic upwelling across its lower boundary in the tropics is balanced closely by cross-isentropic downwelling across its lower boundary in the extra-tropics.

Because mass in the Underworld is extracted mainly from the extra-tropical Middleworld, the extra-tropical Middleworld is characterized by a "mass-deficit", especially in winter. This translates into a low isentropic density in the extra-tropical Middleworld relative to the isentropic density in the tropical Middleworld. While average isentropic density in the tropical Middleworld (equatorward of 30°N) varies very little in time, not departing very much from 80 kg m^{-2}K^{-1} at any time of the year, average isentropic density in the extra-tropical Middleworld,

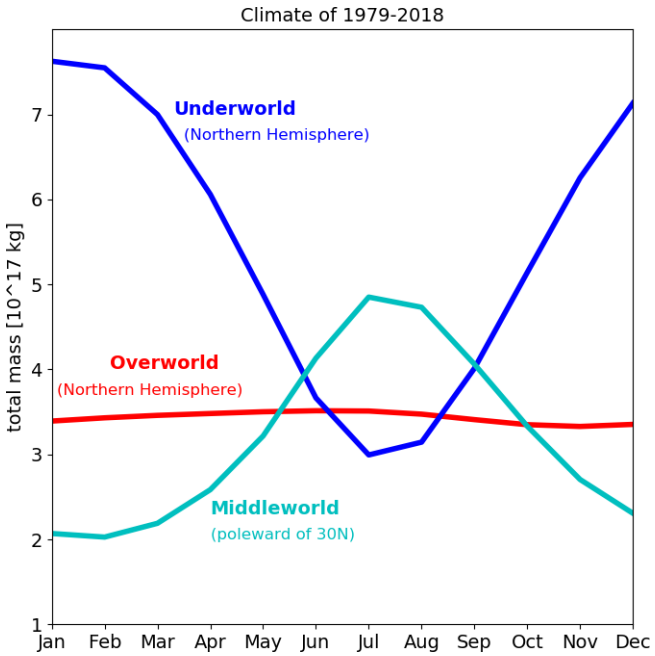

Figure 7. Showing that the Underworld and the extra-tropical Middleworld are communicating vessels. Ensemble mean yearly cycle for the years 1979-2018, of the monthly mean mass in the Northern Hemisphere Underworld ($\theta < 300$ K) (blue), in the Middleworld ($300 < \theta \leq 370$K) poleward of 30°N (cyan), and in the Northern Hemisphere Overworld ($\theta > 370$ K) (red). Based on the ERA-Interim reanalysis (Dee et al., 2011).

poleward of 30°N, undergoes a marked seasonal cycle, decreasing from about 60 $\mathrm{kg\,m^{-2}K^{-1}}$ in summer to 25 $\mathrm{kg\,m^{-2}K^{-1}}$ in winter due to loss of mass to the Underworld.

A step-like change of isentropic density exists between the tropical Middleworld and the extratropical Middleworld. In order to highlight this so-called "σ-step" in a cross section of the zonal-mean state of the atmosphere, we define a reference isentropic density (σ_{ref}) as the area-weighted mean of isentropic density on a specific isentropic level in the Northern Hemisphere. This reference state represents the thermodynamic state in which the mass of the atmosphere is distributed uniformly in the horizontal over the Northern Hemisphere. The difference between actual isentropic density and the isentropic density in the reference state is measured in terms of the zonal-mean normalized (non-dimensional) isentropic density anomaly, defined as

$$\sigma' \equiv \frac{[\sigma] - \sigma_{ref}}{\sigma_{ref}}. \tag{22}$$

Figure 8 shows the monthly mean distributions of $[\sigma]$, σ_{ref} and σ' for January (a) and July (b) as a function of latitude in the Northern Hemisphere (abscissa) and potential temperature (ordinate), derived from the Committee on Space Research International Reference Atmosphere (CIRA) (Fleming et al., 1990). The most interesting feature in Fig. 8 is the negative isentropic density anomaly centered over the North Pole, observed both in January and in July, which translates into a positive extra-tropical PV-anomaly accompanied by a "PV-step" or "PV-front" (Davies and Rossa, 1998) separating high-PV air in the extra-tropics from low-PV air in the tropics at the same isentropic level. The PV-front is found between 30°N and 35°N in January and approximately between 40°N and 45°N in July.

The STJ-core is located close to the PV-front in both months. This can be understood from the "PV-inversion equation", which is an alternative way of expressing zonal-mean thermal wind (Eq. 20). The PV-inversion equation relates the zonal-mean gradient zonal wind velocity to the zonal-mean potential vorticity distribution. The derivation of this equation begins with the definition of zonal-mean potential vorticity:

$$[Z] = \left[\frac{\zeta + f}{\sigma}\right] \approx \frac{[\zeta] + f}{[\sigma]}. \tag{23}$$

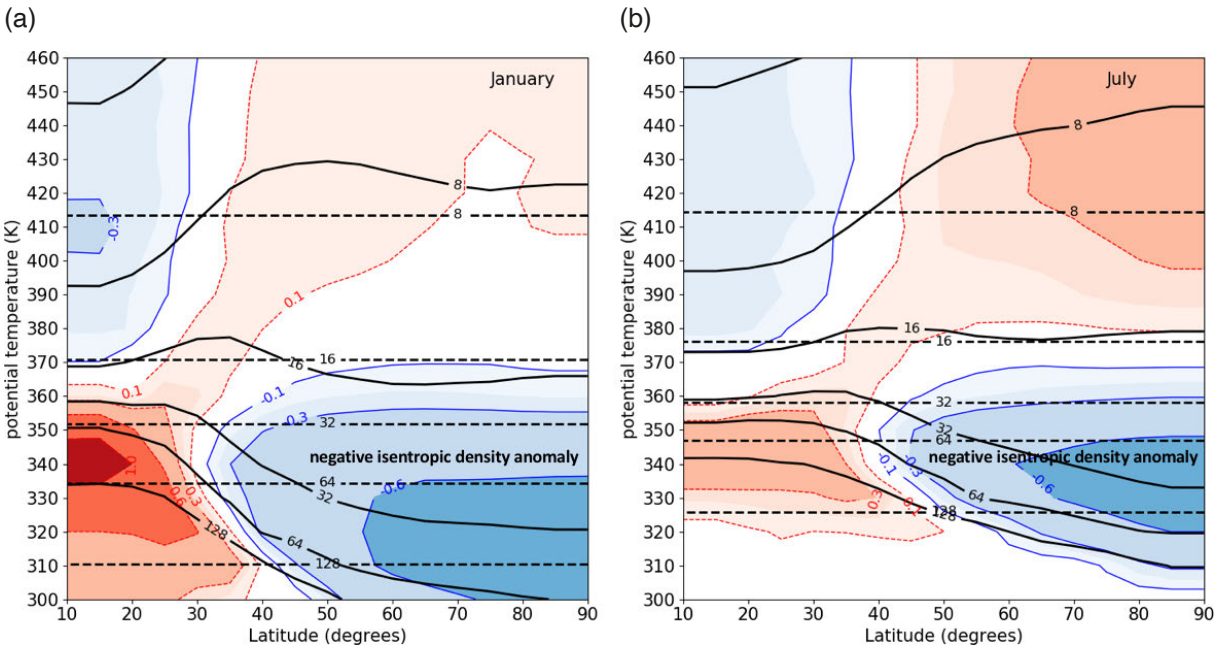

Figure 8. Monthly means zonal-mean isentropic density ([σ]) (solid black lines) and reference isentropic density (σ_{ref}) (dashed black lines), labeled in units of kg m^{-2}K^{-1} for January (a) and July (b) as a function of latitude and potential temperature. Red and blue shading indicates, respectively, a positive and a negative normalized isentropic density anomaly (σ′) (Eq. 22). Contours are drawn at σ′ = −0.6, −0.3, −0.1, + 0.1, + 0.3, + 0.6, + 1. Based on the Committee on Space Research (COSPAR) International Reference Atmosphere (CIRA) (Fleming et al., 1990).

Here [ζ] is the zonal-mean relative vorticity, defined as

$$[\zeta] = \frac{[u]tan\phi}{a} - \frac{\partial[u]}{\partial y}. \tag{24}$$

Differentiating Eq. (23) with respect to y and using the definition of isentropic density (Eq. 3) (assuming that g is a constant) and Eq. (24), the zonal mean thermal wind balance (Eq. 20) is expressed as

$$\frac{\partial}{\partial y}\left(\frac{\partial[u]}{\partial y} - \frac{[u]tan\phi}{a}\right) + \frac{[Z]}{g}\frac{\partial}{\partial\theta}\left(f_{loc}\theta[\rho]\frac{\partial[u]}{\partial\theta}\right) = \beta - [\sigma]\frac{\partial[Z]}{\partial y} \tag{25}$$

with $\beta = df/dy$. All partial derivatives with respect to y in Eq. (25) are performed at constant θ. A simplified version of this so-called "PV-inversion equation" for the special case, f = constant, is derived in the seminal paper by Hoskins et al., (1985) (Eq. (29) in their paper). The PV-inversion equation (Eq. 25) for the case, $f \neq$ constant, i.e. with the β-effect included, was derived and solved first by Hinssen et al. (2010).

If $f_{loc}[Z] > 0$, Eq. (25) is an elliptic partial differential equation. For a given zonal-mean PV-distribution and appropriate boundary conditions on a domain bounded below and above by isentropic surfaces and bounded laterally by the North Pole and by a fixed latitude near the equator (e.g. 10°N), the solution of Eq. (25) yields the "inverted" fields of $[u]$, $[\sigma]$ and $[p]$ (see van Delden and Hinssen, 2012). In other words, both wind – and pressure – (or mass-) fields in a balanced atmosphere are coupled to the PV-distribution. The meridional PV-gradient appears as a prescribed forcing function on the right-hand side of Eq. (25). If this forcing function is equal to zero, i.e. if

$$\beta - [\sigma]\frac{\partial[Z]}{\partial y} = 0, \tag{26}$$

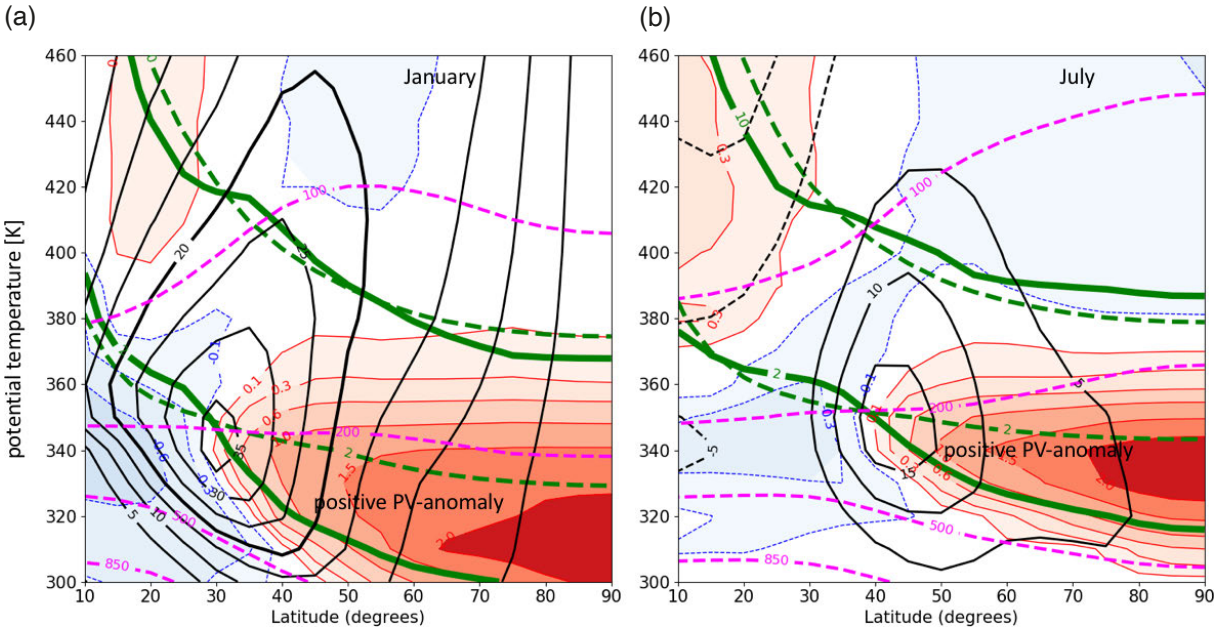

Figure 9. Monthly mean zonal-mean non-dimensional PV-anomaly (red: positive; blue: negative) (contours drawn for $Z^+ = \pm 0.1, \pm 0.3, \pm 0.6, \pm 1, \pm 1.5, \pm 2$), PV (green solid contours) and reference PV (green dashed contours) (only 2 and 10 PVU isopleths are drawn) for January (a) and for July (b) as a function of latitude and potential temperature. Dashed magenta contours represent isopleths of monthly mean $[p]$, labeled in m/s, drawn at 850, 500, 200 and 100 hPa. Black contours represent isopleths of monthly mean $[u]$, labeled in $\mathrm{m\,s^{-1}}$ (contour interval is 5 $\mathrm{m\,s^{-1}}$). Note that the dynamical tropopause (PV = 2 PVU) coincides with the lower and tropical boundary of the positive PV-anomaly. Based on the Committee on Space Research (COSPAR) International Reference Atmosphere (CIRA) (Fleming et al., 1990).

and pressure at the upper and lower isentropic boundary is constant, the solution of Eq. (25) is $[u] = 0$, i.e. the rest state. Therefore, if a reference is defined such that it satisfies Eq. (26), i.e. $[\sigma] = \sigma_{ref}, [Z] = Z_{ref} = f/\sigma_{ref}$ and pressure at the upper and lower isentropic boundary is constant, it would correspond to the balanced state of rest.

Figure 9 shows the monthly mean reference PV (Z_{ref}), the monthly mean zonal-mean PV ($[Z]$) and the associated normalized PV-anomaly in January (a) and in July (b) according to the CIRA. The normalized PV-anomaly is defined in the same way as the normalized isentropic density anomaly (Eq. 22), i.e. as the difference between the observed PV and the reference PV divided by the reference PV. The normalized PV-anomaly is shown in Fig. 9 by red (positive) and blue (negative) shading. The positive extra-tropical PV-anomaly in the lowermost stratosphere, in fact, defines the lowermost stratosphere. It was called *Ex-UTLS PV-anomaly* by Hinssen et al. (2010). *Ex-UTLS* stands for *Extra-tropical Upper Troposphere and Lower Stratosphere*. A more appropriate term is *PV-anomaly of the lowermost stratosphere*. The cyclonic circumpolar circulation is most intense at the equatorward edge of the PV-anomaly of the lowermost stratosphere.

Figure 10 shows the inverted monthly mean fields of $[u]$ and $[p]$ for January (a) and for July (b). The inverted distributions of $[u]$ and $[p]$ strongly resemble the observed distributions of $[u]$ and $[p]$, shown in Fig. 9. This indicates that the monthly mean zonal-mean state is in very close thermal wind balance, which is no surprise in view of Fig. 5.

From the solution of a simplified version of Eq. (25), assuming that f is constant and greater than zero (i.e. for the Northern Hemisphere), Ernst Kleinschmidt (Hoskins et al., 1985; Thorpe, 1993) drew the following three general conclusions, indicating how the vorticity- and mass fields are coupled to each other in an atmosphere in thermal wind balance.

1) *Within an isolated air mass with abnormal potential vorticity, in thermal wind balance, the absolute vorticity deviates from the normal in the same sense as the potential vorticity. The "normal" is identified with the state of rest, i.e. with $Z = Z_{ref}$ and zero thermal wind at the lower boundary.*
2) *Within an isolated air mass with abnormal potential vorticity, in thermal wind balance, the isentropic density deviates from the normal in the opposite sense as the potential vorticity.*

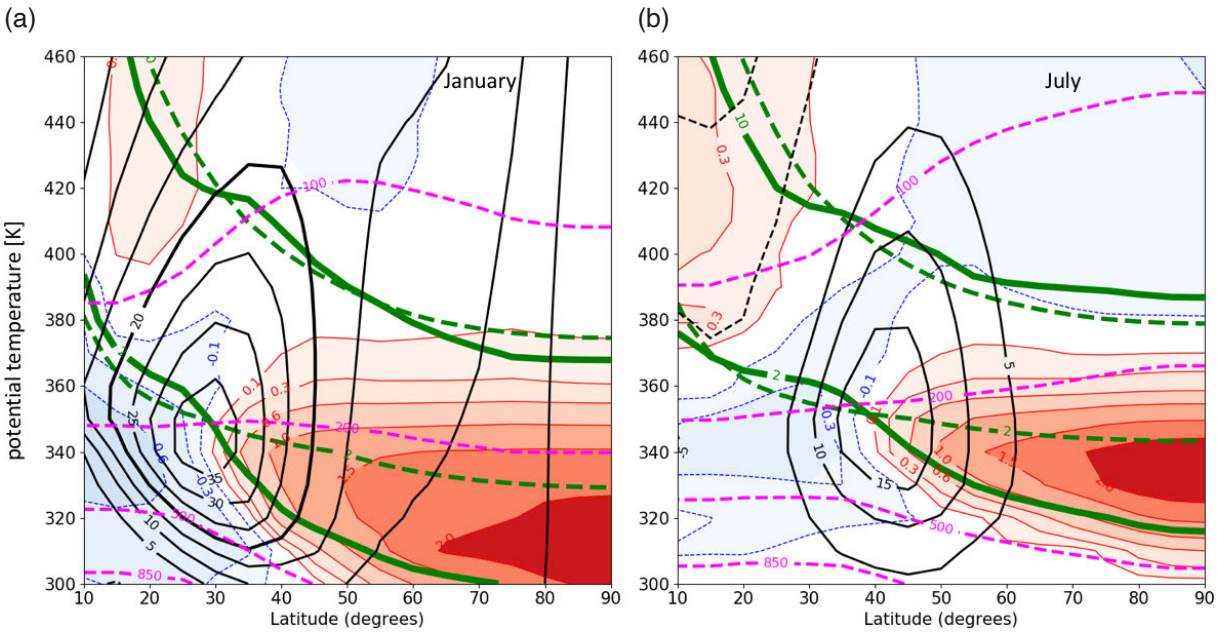

Figure 10. As Fig. 9, except here the black contours represent isopleths of inverted $[u]$ (solution of the PV-inversion Eq. 25) and dashed magenta contours represent isopleths of inverted $[p]$ consistent with the inverted $[u]$ and given the PV-distribution according to the CIRA (Fleming et al., 1990).

3) *Above and below an isolated air mass with abnormal potential vorticity, in thermal wind balance, the isentropic density deviates from the normal in the same sense as the vorticity. Isentropic surfaces are raised below an air mass of relatively high potential vorticity in thermal wind balance. Isentropic surfaces are lowered above an air mass of relatively high potential vorticity in thermal wind balance. Thus, an upper level cyclone has a cold core below and a warm core above the associated potential vorticity anomaly, while an upper level anticyclone has a warm core below and a cold core above the associated potential vorticity anomaly. A cold air mass in thermal wind balance only remains cold as long as there are masses of relatively high potential vorticity above it, or masses of relatively low potential vorticity below it. When this condition is no longer fulfilled, the air sinks down and loses the character of a cold air mass.*

These statements are henceforth referred to as "Kleinschmidt's principles". Kleinschmidt's principles are also valid for case, $\beta > 0$. For example, the consequences of the statement, "an upper level cyclone has a cold core below and a warm core above the associated potential vorticity anomaly" (Kleinschmidt's third principle), are revealed in Fig. 9 and Fig. 10 as an upward (downward) bulge of the isobars above (below) the positive PV-anomaly of the lowermost stratosphere, implying that the Baroclinicity, shown in Fig. 6, is "induced" by the PV-anomaly of the lowermost stratosphere.

Hinssen et al. (2010) demonstrated the existence in January of a second positive zonal-mean PV-anomaly in the stratosphere over the North Pole above $\theta = 500$ K, which induces the stratospheric polar winter vortex. This PV-anomaly is responsible for the downward bulge of both the 100 hPa isobar and the 200 hPa isobar poleward of 50°N, a phenomenon which is not observed in July. The polar stratospheric PV-anomaly, therefore, also affects the baroclinicity in the troposphere and even the surface westerlies (Hinssen et al., 2011).

Changes to the zonal-mean PV-field by either diabatic processes or by "PV-mixing" due to eddies will require a corresponding change of the wind- and mass-distributions, consistent with Kleinschmidt's principles, to maintain zonal-mean thermal wind balance. An interesting and important effect comes into play when $\beta > 0$, implying that reference-PV (Z_{ref}) increases with increasing latitude (Eq. 26). Breaking planetary waves (Scott and Cammas, 2002; Bennedict et al., 2004) mix reference PV, creating a negative PV-anomaly poleward of a positive PV-anomaly. This requires a poleward mass flux, from the positive PV-anomaly to the negative PV-anomaly, in order to maintain zonal-mean thermal wind balance. The observed slow poleward mass flux in the stratosphere, known as the "Brewer Dobson circulation" (Butchart, 2014), is thus explained as a direct consequence of maintenance of zonal-mean thermal wind balance in the presence of meridional PV-mixing by breaking planetary waves in the stratosphere.

6. Link between meridional shifts of mass, baroclinicity and STJ-intensity

Figure 11 demonstrates that STJ-intensity in January is positively correlated with the difference in the area-averaged mass in the Middleworld between the tropics (0-30°N) and the lower middle latitudes (30-50°N). This mass-difference, a bulk measure of baroclinicity at 30°N, varies from 3000 kg m^{-2} to nearly 3500 kg m^{-2}. which represents about one third of the total mass in an atmospheric column! It is no coincidence that this large number corresponds roughly to the size of the Underworld in January, in terms of average mass per unit area.

The seasonal cycle of the mass-deficit of the lowermost stratosphere is foremost a direct consequence of exchange of mass between the Middleworld and the Underworld by radiative flux divergence (van Delden, 2014). This process also determines the average seasonal cycle of bulk baroclinicity. The non-seasonal variability of bulk baroclinicity and STJ-intensity is determined by anomalous isentropic shifts of mass in the Middleworld, where anomalous poleward mass shifts promote the negative NAM-phase, while anomalous equatorward mass shifts promote the positive NAM-phase.

Figure 12 compares the January-mean zonal-mean latitudinal distributions of mass in the Underworld, Middleworld and Overworld in 2007 and 2010. A poleward shift of mass in both the Middleworld and the Overworld is observed in January 2010 relative to January 2007, while an equatorward shift of mass is observed in the Underworld in January 2010 relative to January 2007. Meridional mass-shifts in the extra-tropics represent the response to irreversible isentropic mixing of potential vorticity (PV) by planetary waves. PV-mixing is most intense in the circumpolar planetary waveguide on the poleward side of the baroclinic zone (Branstator, 2002; Manola et al., 2013). A large poleward shift of mass in the Middleworld in January 2010 is consistent with more intense and deeper than normal PV-mixing.

Figure 13 shows cross-sections of the isentropic net meridional mass flux (Eq. 6) for January 2007 (a) and for January 2010 (b). The upper poleward branch of the net mass flux consists of two nearly separate branches (see also Fig. 3): (1) a tropical branch above 320 K, which is part of the cross-equatorial winter Hadley cell, and (2) an extra-tropical branch between 290 K and 320 K poleward of 30°N. The latter branch is most likely driven by meridional PV-mixing due to eddies resulting mostly from baroclinic instability. The border between the two

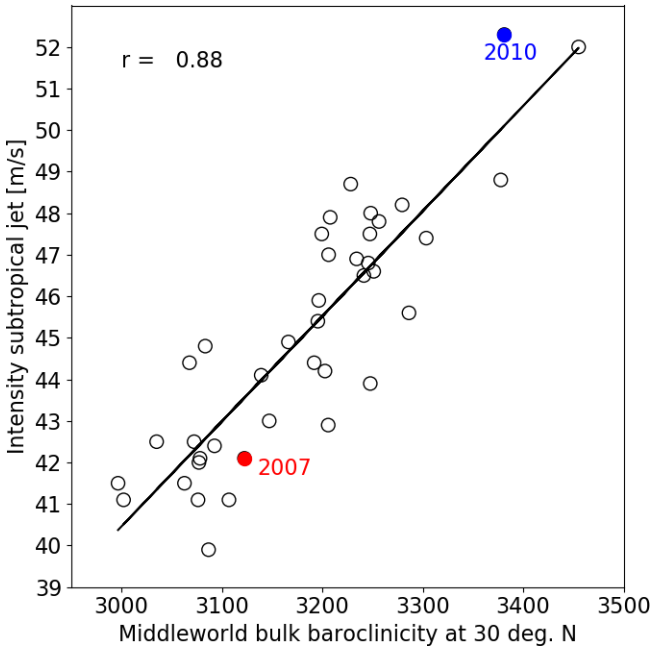

Figure 11. January-mean intensity of the sub-tropical jet (m s^{-1}) at $\theta = 350$ K (see Fig. 2) as a function of January-mean "Middleworld bulk baroclinicity" at 30°N, defined as the difference in the average mass per unit area in the Middleworld, between the tropics (0°-30°N) and the lower middle latitudes (30°N-50°N). Each circle represents a monthly mean value for January in the years 1979-2018. The years 2007 and 2010 are indicated in red and blue, respectively. The black straight line is the best linear fit to the 40 points. The associated correlation coefficient, $r = 0.88$. The standard error of r is < 0.04. Based on the ERA-Interim re-analysis (Dee et al., 2011).

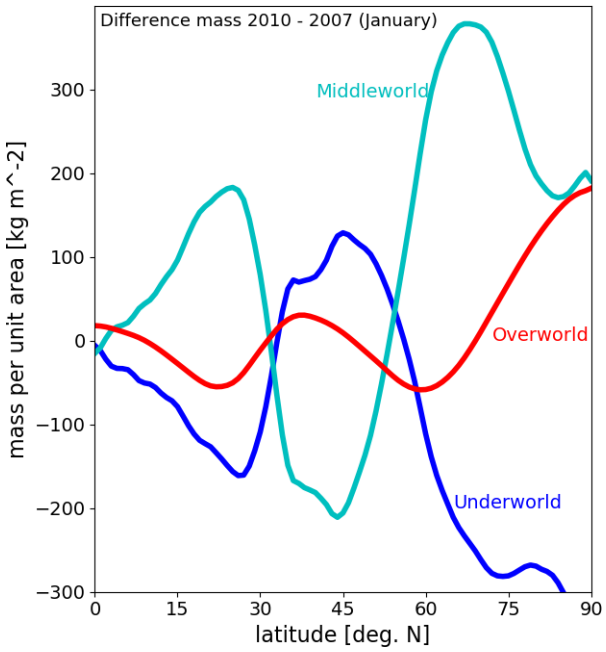

Figure 12. In the negative NAM-phase, mass is shifted poleward in the Middleworld while mass is shifted equatorward in the Underworld, compared to the positive NAM-phase. Monthly-mean and zonal-mean mass difference between January 2010 and January 2007 in the Underworld ($\theta < 300$ K) (blue), Middleworld ($300 \leq q \leq 370$ K) (cyan) and Overworld ($q > 370$ K) (red) as a function of latitude in the Northern Hemisphere. Based on the ERA-Interim re-analysis (Dee et al., 2011).

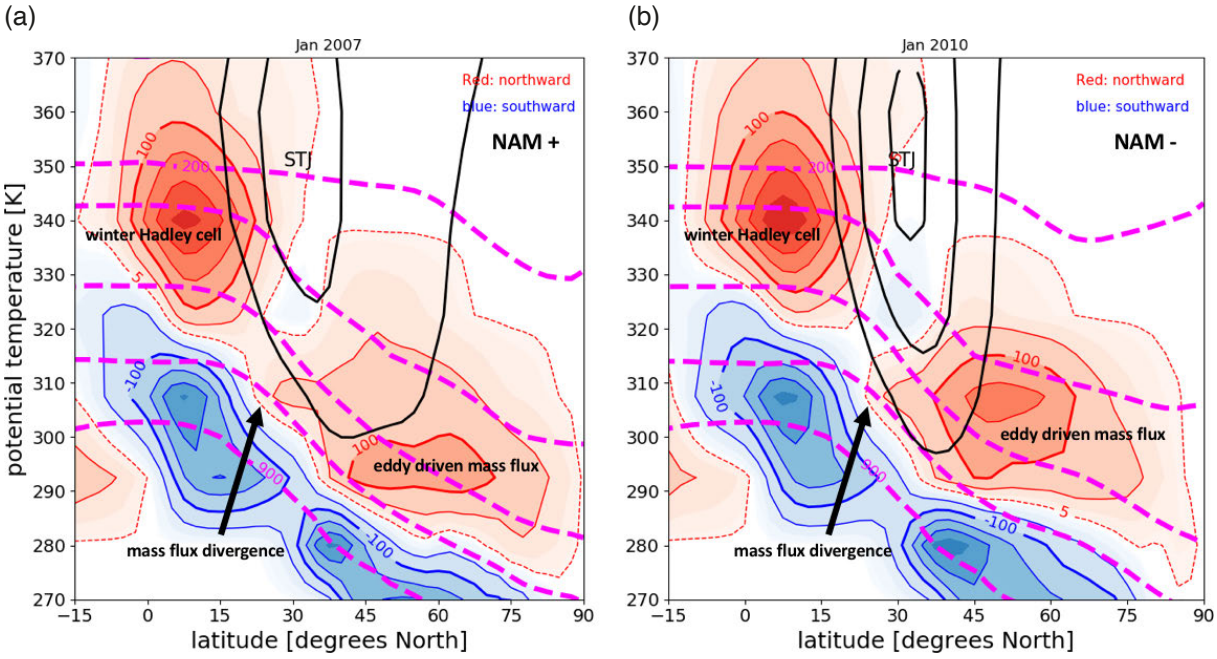

Figure 13. Monthly mean zonal-mean distributions of isentropic meridional mass flux, pressure and zonal wind velocity as a function of potential temperature and latitude, for January 2007 (a) and January 2010 (b). Solid red contours and red shading corresponds to northward mass flux. Solid blue contours and blue shading corresponds to southward mass flux. Solid contours are drawn at intervals of 50 kg s^{-1} K^{-1} per m^{-1}. Shading starts at $\pm$ 5 kg s^{-1} K^{-1} m^{-1} (red dashed contour). Dashed magenta contours represent isopleths of monthly mean $[p] = 900$, 700, 500, 300, and 200 hPa. Solid black contours correspond to isopleths of monthly mean $[u]$ drawn every 15 m s^{-1}. "STJ" stands for "Sub-Tropical Jet". Based on the ERA-Interim reanalysis (Dee et al., 2011).

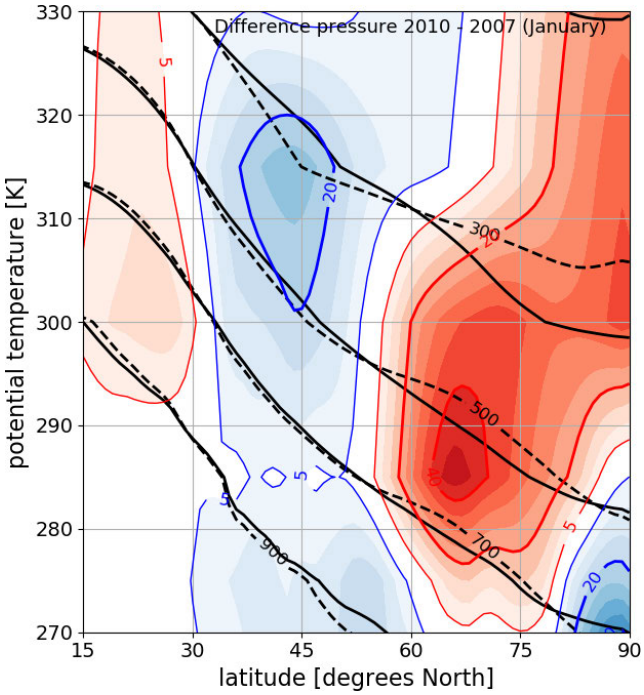

Figure 14. Monthly mean, zonal-mean fields of pressure in January 2007 (solid lines) and in January 2010 (dashed lines), labeled in hPa, and the difference between these two zonal-mean pressure fields, labeled in hPa, where red indicates that pressure is higher in 2010 and blue indicates that pressure is lower in 2010. Based on the ERA-Interim reanalysis (Dee et al., 2011).

branches of the residual circulation coincides with the baroclinic zone and the associated STJ. The core of the baroclinic zone is characterized by a relatively weak meridional isentropic mass flux. Some say that the STJ acts as a "leaky mass transfer barrier" (Esler, 2008), which appears most effective when the STJ is intense.

The eddy driven extra-tropical circulation of mass, on the poleward side of the STJ, is more confined in the meridional direction, and also much deeper and more intense in January 2010 than in January 2007. More than 2×10^{17} kg of air passes the 50°N parallel in poleward direction in the Middleworld in January 2010, while only half this amount passes the same parallel in poleward direction in the Middleworld in January 2007. The total mass of air in the Middleworld, poleward of 50°N, in a typical month of January is about 0.8×10^{17} kg. This reservoir of mass is replaced more than twice in January 2010 and only once in January 2007. The air mass, converging over the polar cap in the Middleworld, contributes to an increase of the isentropic pressure in a ring around the North Pole, as can be seen Fig. 14.

Figure 15 demonstrates that STJ-intensity and isentropic mass flux divergence in the Middleworld, between 30°N and 50°N, are positively correlated. In other words, a relatively intense STJ is associated with a relatively *weak* poleward isentropic mass flux at 30°N in the Middleworld and a simultaneous relatively *intense* poleward isentropic mass flux at 50°N in the Middleworld. In view of Fig. 11 and Fig. 15, we may conclude that mass flux divergence between 30°N and 50°N supports or strengthens the baroclinicity in this latitude band and the STJ, which, in turn, promotes the formation of eddies by baroclinic instability, which carry mass poleward. Thus, a feedback loop exists between baroclinicity, STJ-intensity and mass flux divergence. This feedback-loop is likely an important factor in contributing to the persistence of the negative NAM-phase.

7. Sea-level pressure distribution in the Northern Hemisphere

How is the variability of the isentropic meridional mass flux, illustrated in Fig. 13, reflected in the zonal-mean distribution of pressure at sea level and in the surface westerlies? This section paves the way to the answer to this question, which will come in section 8. First, a short overview is given of the synoptic meteorology of the distribution of sea-level pressure and the associated near surface winds in the Northern Hemisphere.

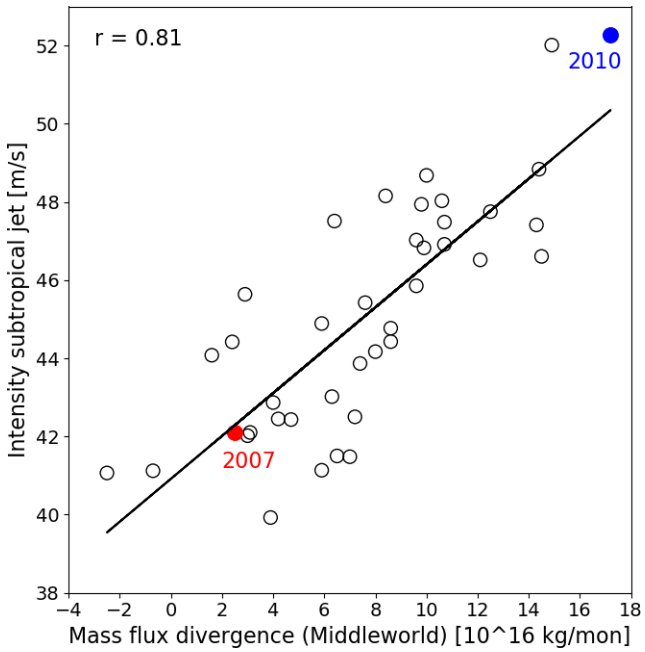

Figure 15. Showing that monthly mean STJ-intensity at $\theta = 350$ K (ordinate) is positively correlated with monthly mean mass flux divergence between 30°N and 50°N in the Middleworld (abscissa). Mass flux divergence is defined as the zonal-mean isentropic meridional mass flux at 50°N minus the zonal-mean isentropic meridional mass flux at 30° between 300 K and 370 K. Each circle represents a monthly mean value for January in the years 1979-2018. The black solid line represents the best linear fit to the 40 points (correlation coefficient, $r = 0.81 \pm 0.05$). January 2007 (red) and January 2010 (blue) are indicated explicitly. Based on the ERA-Interim reanalysis (Dee et al., 2011).

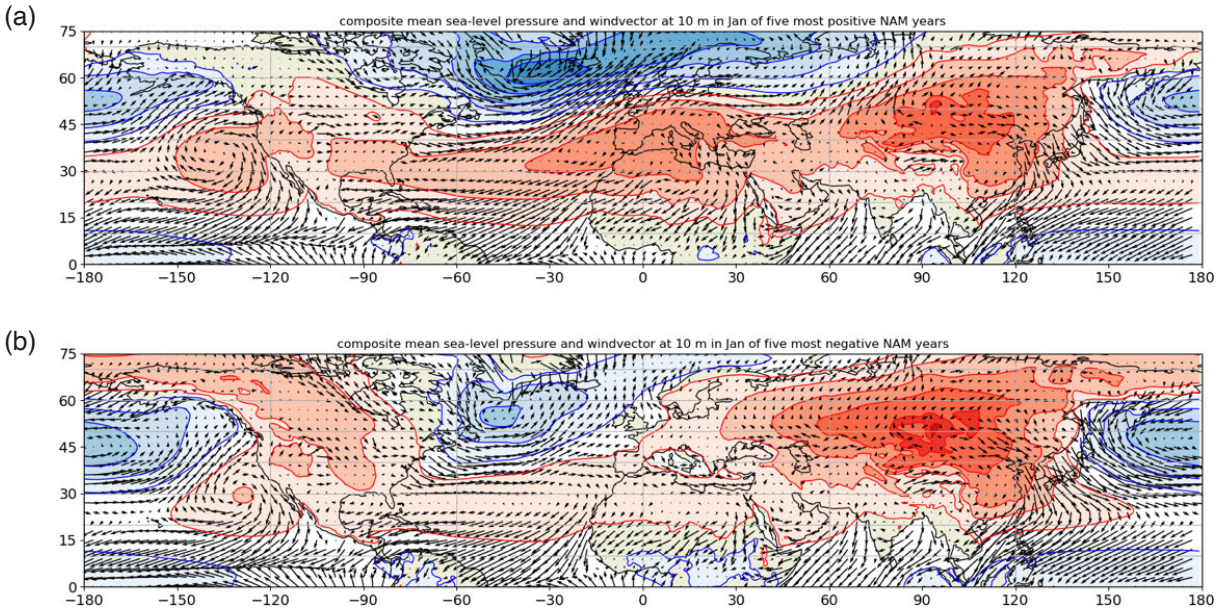

Figure 16. Composite-mean monthly mean distributions of pressure at sea-level and wind vector at 10 m above the earth's surface for the five months of January with the most positive monthly mean NAM-index and for the five months of January with the most negative NAM-index (b) (see also Fig. 21). The NAM-index is defined in section 8. Contour interval is 5 hPa; red shading corresponds to $p > 1015$ hPa; blue shading corresponds to $p < 1010$ hPa. The length of the arrow is proportional to the wind velocity. Latitude (vertical axis) and longitude (horizontal axis) are indicated in degrees. Based on the ERA-Interim re-analysis (Dee et al., 2011).

Zonal-mean sea-level pressure in the middle latitudes in winter is determined by oceanic lows and by continental highs at similar latitudes. A very prominent continental high in winter is the "Eurasian high" over Central Asia (Fig. 16). It is typical for the negative NAM-phase that the Eurasian high extends further northward and westward towards Scandinavia than it does in the positive NAM-phase. Another continental high is observed in winter over Canada. This high is connected to the Eurasian high via Alaska. This connection is much stronger in the negative NAM-phase than in the positive NAM-phase.

The oceanic "subpolar lows" are known as the "Iceland low" and the "Aleutian low". These are climatic manifestations of the "storm tracks" over, respectively, the Atlantic and Pacific Oceans, manifest as a string of intense cyclones moving eastward or north-eastward in a latitude-band roughly between 35°N and 65°N from the genesis regions on the western side of the oceans. In January 2010 the storm tracks and the associated surface westerlies are shifted to lower latitudes over both oceans, while surface westerlies are practically absent over the northern continents.

Zonal-mean sea-level pressure between 30 and 40°N is relatively high due to the presence of oceanic sub-tropical highs. The Azores high over the Atlantic Ocean and the North Pacific high, west of California, are the most prominent sub-tropical highs in the Northern Hemisphere (Fig. 16). They are much more intense in the positive NAM-phase than in the negative NAM-phase. The Azores high also extends far eastward over Northern Africa and into the area of the Mediterranean Sea in the positive NAM-phase, while relatively low sea-level pressure prevails over the Mediterranean Sea in the negative NAM-phase.

The continental highs in winter are formed due to high-latitude convergence of the poleward isentropic mass flux in the upper branch of the extra-tropical residual circulation at isentropic levels between $\theta = 290$ K and 320 K (Fig. 13). Due to cross-isentropic downwelling, this air mass is collected and imprisoned in the Underworld over the Arctic and the continents of Eurasia and North America. This is reflected in a rise of zonal-mean sea-level pressure at high northern latitudes from the end of summer until mid-spring of the next year (Fig. 17).

The synoptic variability of sea-level pressure is quite complicated, but we can, by restricting our attention to sea-level pressure in the annular belts of action (Fig. 17), simplify matters considerably. Zonal-mean sea-level pressure in the two "annular belts of action", at or close to 35°N and 65°N, co-vary on a seasonal time scale consisting of three seasonal phases (Fig. 18). These three seasonal phases are discussed in the following.

In phase 1 (August-November) the Northern Hemisphere cools, due to decreasing insolation, while the Southern Hemisphere warms due to increasing insolation. Isobaric surfaces in the Southern Hemisphere are raised relative to those in the Northern Hemisphere. This results in a negative northward (cross-equatorial) pressure gradient, especially at greater heights, which induces a net northward (cross-equatorial) transfer of mass, leading to a pressure rise at sea-level at all latitudes in the Northern Hemisphere. Shaw (1931), who was the first to understand the importance of this effect, estimated that the atmosphere in the Northern Hemisphere gains about 10^{16} kg between mid-July and mid-January. This air mass crosses the equator into the Northern Hemisphere, via the upper branch of the winter Hadley cell in the layer between $\theta = 320$ and $\theta = 360$ K (Fig. 13) and descends to lower isentropic levels in the subtropics (Fig. 3). Upon reaching levels between $\theta = 290$ K and $\theta = 310$ K, part of this air mass is absorbed by the return flow of the Hadley cell, returning to the opposite hemisphere, while a relatively small part is absorbed by middle latitude eddies and transferred across the afore-mentioned "leaky mass transfer barrier" into the extra-tropical Middleworld. The latter air-mass is ultimately collected into the Underworld and further into the Lower Underworld, defined as the atmosphere below $\theta = 275$ K. The Lower Underworld might be called the "cellar of the atmosphere". The mass in the Lower Underworld in the Northern Hemisphere increases from barely 10^{16} kg in mid-July to 15×10^{16} kg in mid-January. Therefore, the mass gain in the Lower Underworld exceeds the mass loss of the Southern hemisphere to the Northern Hemisphere by a factor 15, which implies that most of the mass in the Lower Underworld in the Northern Hemisphere comes from the Northern Hemisphere itself, notably from the Middleworld poleward of 30°N, as can be inferred from Fig. 7.

In phase 2 (December-March), sea-level pressure at high latitudes continues to rise, presumably due to the intense eddy driven poleward mass flux between 290 K and 315 K in the middle latitudes. The associated relatively strong isentropic mass flux divergence in the northern horse latitudes (just poleward of 30°N) leads to a decrease of *sea-level* pressure in the subtropics, which leads to a weakening of the meridional gradient of sea-level pressure across the middle latitudes, and also leads to a weakening of the zonal-mean surface-westerlies in late winter and spring (Fig. 1a). Phase 2 represents the climatological analogue of a transition from the positive NAM phase to the negative NAM phase. Indeed, during phase 2 we observe an equatorward shift of the surface westerlies and an intensification of the STJ (Fig. 1), which is consistent with such a transition.

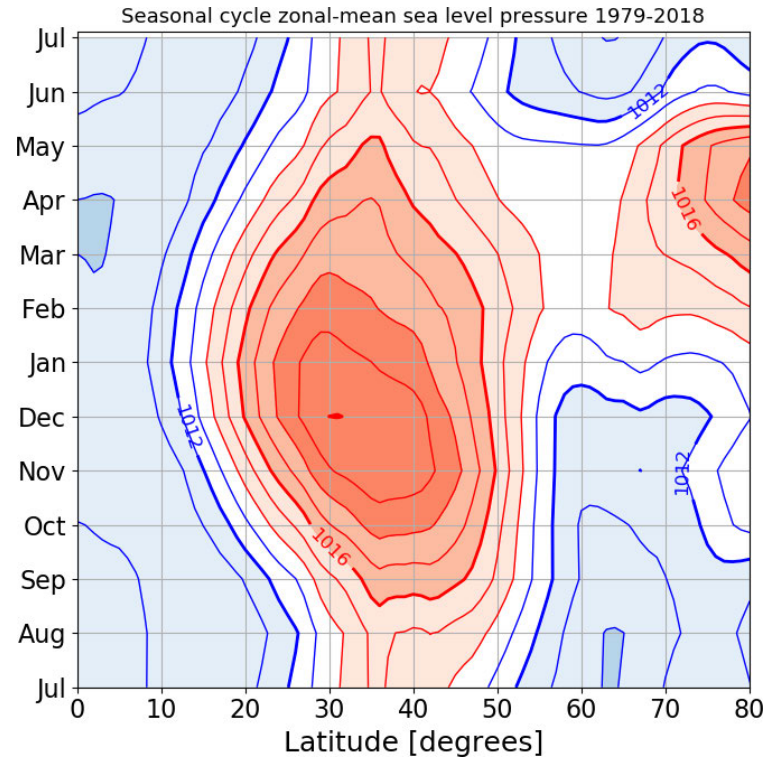

Figure 17. Ensemble mean (for the years 1979-2018) seasonal cycle of the monthly mean zonal-mean sea-level pressure, [*p*], as a function of month (ordinate) and latitude (abscissa). Contours are drawn at 1 hPa intervals. Blue contours correspond to [*p*] ≤ 1013 hPa; red contours correspond to [*p*] ≥ 1014 hPa. Red shading indicates high sea-level pressure (x ≥ 1014 hPa). Blue shading indicates low sea-level pressure (≤ 1012 hPa). Based on the ERA-Interim reanalysis (Dee et al., 2011). A similar analysis was published by Christie and Trenberth (1985) (their Fig. 1a). The two middle latitude annular belts of action are recognized as a belt of relatively high pressure around 35°N and a belt of relatively low pressure at 65°N.

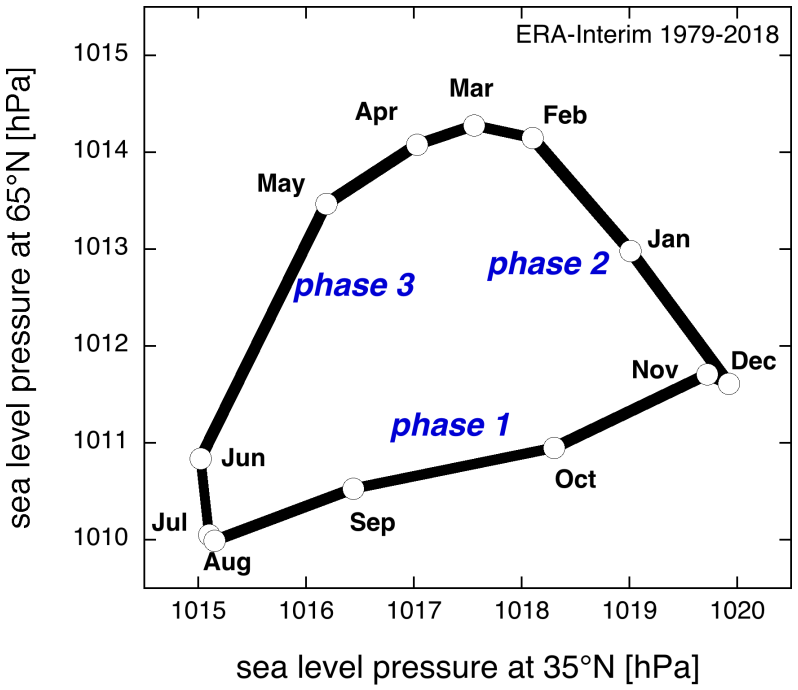

Figure 18. Showing the three *seasonal phases* in the annual march of the ensemble monthly mean zonal-mean sea-level pressure at 35°N and at 65°N, for the years 1979-2018. Based on the ERA-Interim re-analysis (Dee et al., 2011).

In phase 3, (April-July), zonal mean sea-level pressure decreases in *both* Northern Hemisphere annular belts of action, under influence of increasing solar irradiance. Decreasing albedo due to quick disappearance of snow-cover over Eurasia and North America, especially in April and May, leads to more absorption by the Earth's surface of solar radiation, a strong rise in temperature of the land surface and a simultaneous warming of the lower atmosphere, manifest as *net* cross-isentropic *upwelling* over land. Moreover, due to decreasing baroclinic eddy activity, the middle latitude eddy-driven poleward mass flux in the Middleworld layer between $\theta = 290$ K and $\theta = 320$ K of the Northern Hemisphere nearly ceases.

8. A surface NAM-index and its link to the residual circulation

Figure 19 demonstrates that January-mean zonal-mean sea-level pressure anomalies in the annular belts of action are anti-correlated. January 2007 (positive phase of the NAM; weak mass exchange) and January 2010 (negative phase of the NAM; strong mass exchange) are at the opposite ends of the relatively broad distributions of monthly mean sea-level pressures in the respective annular belts (relative to the climate, shown in Fig. 18).

Felix Exner (1914) was the first to show that sea-level pressure variability at high latitudes is anti-correlated with sea-level pressure variability at sub-tropical latitudes. Several decades later Edward Lorenz correlated the zonal-mean and monthly mean sea-level pressure anomalies for *all* latitude-combinations between 15°N and 75°N separated at 10° intervals, using observations for the years 1932-1939. Lorenz (1951) concluded that the Northern Hemisphere "*tends to contain two homogeneous zones, centered near 70°N and 35°N, separated by a transition zone near 50°N. Pressures within either homogeneous zone tend to be correlated positively with other pressures in the same zone and negatively with pressures in the other zone, while pressures within the transition zone tend to be uncorrelated with other pressures*".

Using the NCEP reanalysis data for the years 1958-2000, Li and Wang (2003) confirmed Lorenz's findings. Figure 20 shows the result of a similar analysis using ERA-Interim reanalysis data for January 1979-2018. The outstanding feature in this figure is the relatively large negative correlation between the anomalies of zonal-mean

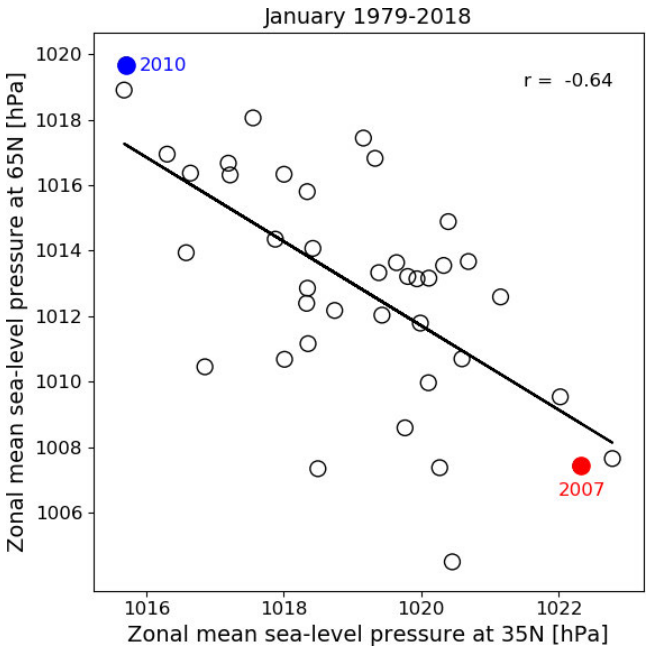

Figure 19. January ensemble mean zonal-mean sea-level pressure at 35°N and at 65°N, for the years 1979-2018. The correlation coefficient, r, is -0.64 ± 0.09. Positive pressure anomalies at low latitudes are associated with negative pressure anomalies at high latitudes and vice versa. Two extreme NAM-phase months are indicated in red (2007: positive NAM-phase) and blue (2010: negative NAM-phase). The NAM-index is defined in section 6. The January-mean zonal-mean sea-level pressure in years 1979-2018 is 1012.7 hPa at 65°N and 1019 hPa at 35°N. Based on the ERA-Interim re-analysis (Dee et al., 2011).

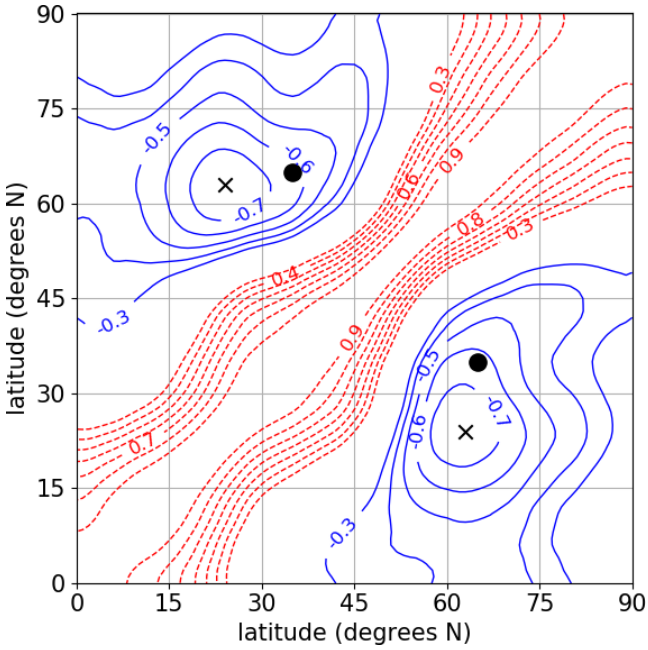

Figure 20. Correlation coefficient between January-mean zonal-mean sea-level pressure anomalies for different latitude combinations in the Northern Hemisphere (1979-2018). The contour interval is 0.1 (absolute values lower than 0.3 ± 0.14 are not contoured). Solid blue lines indicate a negative correlation. Dashed red lines indicate positive correlation. The cross indicates the latitude-combination (24°N, 63°N) of highest anti-correlation (-0.78 ± 0.06) in January. The dot indicates the latitude-combination (35°N, 65°N) of highest "yearly-mean" anti-correlation according to a similar analysis by Li and Wang (2003). Based on the ERA-Interim reanalysis (Dee et al., 2011).

sea-level pressure in the subtropics and the anomalies of zonal-mean sea-level pressure at subpolar latitudes. The largest negative correlation in January (-0.78 ± 0.06) is found for the combination 24°N and 63°N.

The latitude-combination of largest negative correlation varies from month to month. Li and Wang (2003) performed this correlation analysis for all months and found that the "annual mean" largest *negative* correlation coefficient between sea-level zonal mean pressure anomalies with respect to the long-term average seasonal cycle in the Northern Hemisphere occurs for a latitude-combination of 35°N and 65°N. On the basis of this result, Li and Wang (2003) proposed a "Northern Annular Mode Index", or "NAM Index", defined as the anomalous *difference* of the monthly mean zonal mean sea-level pressure between 35°N and 65°N, normalized with the standard deviation of this difference.

Figure 21 shows the January-mean NAM Index, defined in accordance with Li and Wang (2003), as function of the January-mean divergence of the poleward isentropic mass flux in the Middleworld between 50°N and 30°N. Again, January 2007 and January 2010 are at the opposite extremes of the distribution of both variables. While the latter variable is positively correlated with the intensity of the STJ (Fig. 15), it is apparently anti-correlated with the NAM Index. The physical explanation of this anti-correlation is simply that divergence of the poleward isentropic mass flux in the Middleworld in the latitude band between 30°N and 50°N leads to a decrease of sea-level pressure in this latitude band and a simultaneous increase of sea-level pressure at higher latitudes, that is a reduction of the meridional gradient of zonal-mean sea-level pressure in the middle latitudes (between 35°N and 65°N).

Air masses generally descend into the Underworld over the cold continents. The cold air in the Underworld cannot easily escape to lower latitudes, especially not over Asia, due to the presence of blocking mountain barriers to the south, such as the Tibetan Plateau and surrounding mountains. The principal escape route out of the Underworld is by outbreaks of cold air in connection with intense cyclone activity (Kanno et al., 2015), especially over the West Pacific and West Atlantic Oceans where frequent intense cross-isentropic upwelling at $\theta = 300$ K occurs (see Fig. 4a of Iwasaki et al., 2014). Polar air outbreaks are principal contributors to the lower equatorward branch of the meridional circulation of mass (Fig. 13). Although high-latitude mass flux convergence in the Middleworld is countered by high-latitude mass flux divergence in the Underworld, the mass flux divergence in the Underworld is generally not fast enough to directly cancel the mass flux convergence in the Middleworld, as was also shown by Yu et al. (2015).

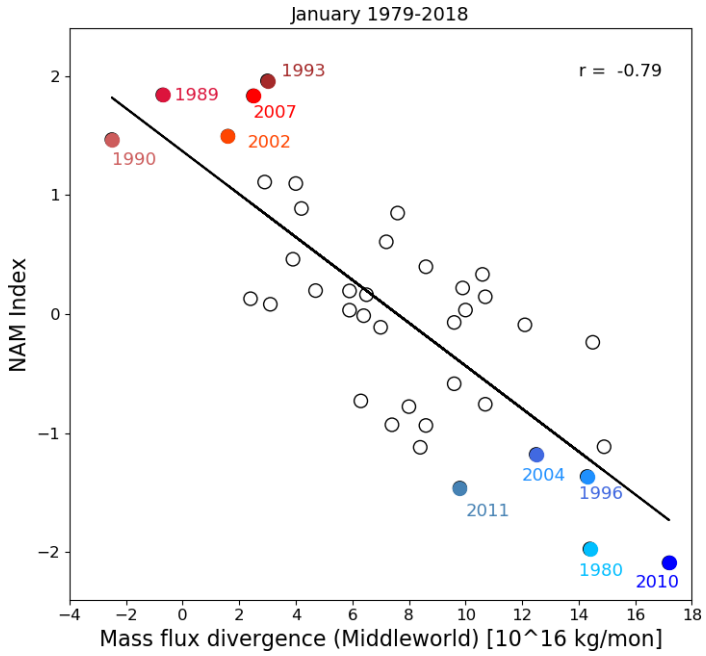

Figure 21. The January-mean NAM-index (ordinate) as a function of the January-mean divergence of the isentropic zonal-mean mass flux between 30°N and 50°N in the Middleworld (abscissa), for the years 1979-2018. The straight solid line is the best linear fit (correlation coefficient, $r = -0.79 \pm 0.06$). The five months used to construct the composites shown in Fig. 16, are indicated explicitly in blue (lowest NAM-index) and red (highest NAM-index). Based on the ERA-Interim reanalysis (Dee et al., 2011).

In how far does the surface NAM-index, defined in this section, represent a mode of variability in which nearly synchronous sea-level pressure oscillations occur at all longitudes within an annular belt of action? This question has been the subject of discussion and debate at least since the beginning of this century (Wallace, 2000; Deser, 2000; Ambaum et al., 2001; Vallis and Gerber, 2008; Gerber and Thompson, 2017). As a contribution to resolving this discussion, Fig. 22 shows the correlation coefficient (r) between the January-mean sea-level pressure and the January-mean NAM Index, as defined earlier in this section. It is not difficult to recognise the two Northern

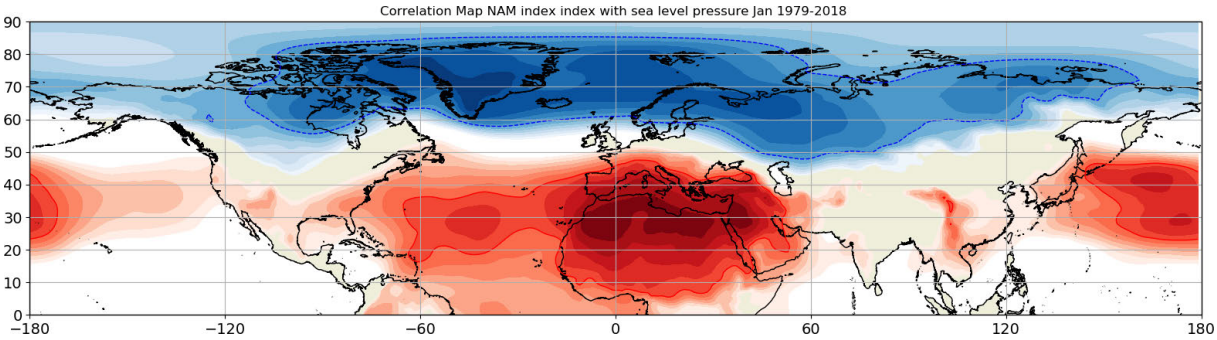

Figure 22. Showing that the NAM-index represents a mode of variability in which approximately synchronous sea-level pressure oscillations occur at all longitudes within an "annular belt of action". Distribution of the correlation coefficient (r) between the January-mean sea-level pressure and the January-mean NAM Index at every grid point for the period 1979-2018. Red shading indicates positive a correlation coefficients larger than 0.2, while blue shading indicates negative correlation coefficients, smaller than −0.2. The $r = -0.5 \pm 0.12$ and $r = +0.5 \pm 0.12$ isopleths are indicated by the dashed lines. Correlation coefficients larger than 0.5 are observed in sub-tropical annular belt of action over the Atlantic Ocean, Southern Europe and Northern Africa, and over the Western Pacific Ocean. The abscissa corresponds to longitude; the ordinate corresponds to latitude, indicated in degrees. Based on the ERA-Interim reanalysis (Dee et al., 2011).

Hemisphere annular belts of action. The subpolar annular belt poleward of about 60°N (blue shading) is much more zonally symmetric than the sub-tropical annular belt roughly between 20°N and 50°N (red shading), which is interrupted over the Eastern Pacific Ocean and adjacent North America, and over South East Asia. Nevertheless, there is a clear signal of a sub-tropical annular belt of action, not only over the Atlantic sector, including Northern Africa and the Mediterranean Sea, but also over the Western Pacific Ocean. This may indicate that the poleward mass flux in the Middleworld, which drives the NAM at sea-level into its negative phase (Fig. 20), occurs at preferred longitudes in connection with the phase of stationary planetary waves. It may also indicate that the source region of storms in, respectively, the West Pacific and the West Atlantic Oceans are connected on a monthly time scale. These topics will be addressed in part 2 of this paper (van Delden, 2024).

9. Concluding remarks

The negative phase of the Northern Annular Mode (NAM) is characterized by an intense zonal-mean sub-tropical jet (STJ), linked to intense zonal-mean baroclinicity at the poleward edge of the subtropics (Fig. 2, Fig. 6 and Fig. 13), induced by a positive PV-anomaly in the lowermost stratosphere, with its "center of gravity" shifted to lower than average latitudes due to a poleward eddy-driven shift of mass (Fig. 12, Fig. 13 and Fig. 14). All these features are linked in the following positive feedback-loop. Intense zonal-mean baroclinicity in the subtropics leads to baroclinic instability of planetary waves, forming eddies, which propagate on a relatively narrow circumpolar waveguide just poleward of the STJ. These eddies mix potential vorticity (PV) on isentropic surfaces, thereby reducing the characteristic positive poleward PV-gradient in the wave guide. Simultaneous maintenance of zonal-mean thermal wind balance (Fig. 4) requires a poleward isentropic mass flux in the PV-mixing zone (section 5). Divergence of this mass flux at the equatorward boundary of the PV-mixing zone in the lower middle latitudes in the Middleworld supports or even intensifies the zonal-mean baroclinicity there, which promotes the formation of new eddies and further PV-mixing, maintaining the poleward mass flux and the associated mass flux divergence in the Middleworld. An important undiscussed element in this feedback loop is cross-isentropic downwelling, occuring at high latitudes, which tends to restore the meridional PV-gradient, but is also too weak or slow to eliminate the anomalous eddy-driven poleward mass-shift in the Middleworld (Fig. 12).

How does the atmosphere reach this self-maintained state in the first place? How is the extra-tropical atmosphere "pushed" out of the positive or neutral NAM-phase into the extreme negative NAM-phase, or vice versa? This "push" might come from deep convection in the tropics (Riviere and Drouard, 2015), from the stratosphere (Baldwin and Dunkerton, 2001; Hinssen et al., 2011), from the ocean (Li et al., 2010), from a change in the intensity of cross-isentropic upwelling into the Middleworld, associated with polar air outbreaks over relatively warm ocean surfaces (Yu et al., 2015) or from a change of seasons (Baldwin et al., 2003).

Part 2 of this paper (van Delden, 2024) addresses the following questions. What features of the general circulation of the atmosphere should we observe to characterize and understand the persistence of the positive NAM-phase? What processes break the feedback loop which maintains the NAM in its negative phase? The zonal-mean westerlies are the result of a process of mutual adjustment of the zonal-mean distributions of mass *and* vorticity to maintain *zonal-mean* thermal wind balance in the presence of eddies, which, by mixing of PV, disturb this state of balance. While the persistence of the negative NAM-phase is linked to a positive feedback-loop associated with the zonal-mean distribution of mass, as is explained in the present paper, the persistence of the positive NAM-phase is linked to a positive feedback-loop associated in first place with the zonal-mean distribution of vorticity.

Acknowledgments. This paper is a follow-up of a workshop on the Northern Annular Mode held at IMAU (Utrecht University) on 19 April 2018. I thank the presenters (Maarten Ambaum, Frank Selten, Annalisa Cherchi, Wim Verkley, Wim van Caspel and Bob Ammerlaan) for their presentations and all participants for their contributions to discussions. I thank Angelo Bohan for suggesting the term "Kleinschmidt's principles" (section 5).

References

Ambaum, M. H. P., B. Hoskins and D. B. Stephenson (2001). Arctic oscillation or North Atlantic oscillation?, J. Clim., 14, 3495-3507, doi:10.1175/1520-0442(2001)014<3495:AOONAO>2.0.CO;2.

Ambaum, M. H. P. (1997). Isentropic formation of the tropopause, J. Atmos. Sci., 54, 555-568, doi:10.1175/1520-0469(1997)054<0555:IFOTT>2.0.CO;2.

Appenzeller, C., J. R. Holton and K. H. Rosenlof (1996). Seasonal variation of mass transport across the tropopause, J. Geophys. Res., 101, 15071-15078, doi:10.1029/96JD00821.

Baldwin, M. P. (2001). Annular modes in global daily atmospheric surface pressure, Geophys. Res. Lett., 28, 4115-4118, doi:10.1029/2001GL013564.

Baldwin, M. P. and T. J. Dunkerton (2001). Stratospheric Harbingers of Anomalous Weather Regimes, Science, 294, 581-584, doi:10.1126/science.1063315.

Baldwin, M. P., D. B. Stephenson, D. Thompson, W. J. Dunkerton et al. (2003). Stratospheric Memory and Skill of Extended-Range Weather Forecasts, Science, 301, 5633, 636-640, doi:10.1126/science.108714.

Bennedict, J. J., S. Lee and S. B. Feldstein (2004). Synoptic view of the North Atlantic Oscillation, J. Atmos. Sci., 61, 121-144, doi:10.1175/1520-0469(2004)061<0121:SVOTNA>2.0.CO;2.

Branstator, G. (2002). Circumglobal Teleconnections, the Jet Stream Waveguide, and the North Atlantic Oscillation, J. Clim., 15, 1893-1910, doi:10.1175/1520-0442(2002)015<1893:CTTJSW>2.0.CO;2.

Butchart, N. (2014). The Brewer-Dobson circulation, Rev. Geophys., 52, 157-184, doi:10.1002/2013RG000448.

Cai, M. and C. S. Shin (2014). A Total Flow Perspective of Atmospheric Mass and Angular Momentum Circulations: Boreal Winter Mean State, J. Atmos. Sci., 71, 2244-2263, doi:10.1175/JAS-D-13-0175.1.

Cattiaux, J. R., C. Vautard, P. Cassou, V. You et al. (2010). Winter 2010 in Europe: a cold extreme in a warming winter, Geophys. Res. Lett, L20704, doi:10.1029/2010GL044613.

Christie, J. R. and K. E. Trenberth (1985). Hemispheric interannual fluctuations in the distribution of atmospheric mass, J. Geophys. Res., 90, 8053-8065, doi:10.1029/JD090iD05p08053.

Davies, H. C. and A. M. Rossa (1998). PV Frontogenesis and Upper-Tropospheric Fronts, Mon. Wea. Rev., 126, 1528-1539, doi:10.1175/1520-0493(1998)126<1528:PFAUTF>2.0.CO;2.

Dee, D., S. M. Uppalaa, A. J. Simmons, P. Berrisford et al. (2011). The ERA-Interim reanalysis: configuration and performance of the data assimilation system, Quart. J. R. Met. Soc., 137, 553-597, doi:10.1002/qj.828.

Delden, A. J. van (1999). The slope of isentropes constituting a frontal zone, Tellus, A, 51, 603-611, doi:10.3402/tellusa.v51i5.14479.

Delden, A. J. van (2000). Linear dynamics of hydrostatic adjustment to horizontally homogeneous heating, Tellus, A, 52, 380-390, doi:10.3402/tellusa.v52i4.12270.

Delden, A. J. van and Y. B. L. Hinssen (2012). PV-theta view of the zonal mean state of the atmosphere, Tellus, A, 64, 18710, doi:10.3402/tellusa.v64i0.18710.

Delden, A. J. van (2014). PV-theta view of diabatic-dynamical interaction in the general circulation, Tellus A, 66, 24880, doi:10.3402/tellusa.v66.24880.

Delden, A. J. van (2024). Physics of the Northern Annular Mode – Part 2: connection to meridional vorticity transfer, Ann. Geophys., doi:10.4401/ag-9024.

Deser, C. (2000). On the teleconnectivity of the Arctic Oscillation, Geophys. Res. Lett, 27, 779-782, doi:10.1029/1999GL010945.

Dessler, A. E., E. J. Hintsa, E. M. Weinstock, J. G. Anderson et al. (1995). Mechanisms controlling water vapor in the lower stratosphere: a tale of two stratospheres, J. Geophys. Res, 100, D11, 23167-23172, doi:10.1029/95JD02455.

Esler, J. G. (2008). Robust and leaky transport barriers in unstable baroclinic flows, Phys. Fluids, 20, 116602, doi:10.1063/1.3013631.

Exner, F. (1914). Über monatliche Witterungsanomalien auf der nördlichen Halbkugel im Winter (On monthly weather anomalies in the Northern Hemisphere in winter), Meteorol. Z., 31, 104-109, translated and edited by E. Volken and S. Brönnimann, Meteorol. Z., 24, 2015, doi:10.1127/metz/2015/0654.

Fink, A. H., T. Brücher, V. Ermert, A. Krüger et al. (2009). The European storm Kyrill in January 2007: synoptic evolution, meteorological impacts and some considerations with respect to climate change, Nat. Hazards Earth Syst. Sci., 9, 405-423, www.nat-hazards-earth-syst-sci.net/9/405/2009/.

Fleming, E. L., S. Chandra, J. J. Barnett and M. Corney (1990). Zonal Mean Temperature, Pressure, Zonal Wind and Geopotential Height as Functions of Latitude, Adv. Space Res., 10, 12, 11-59, doi:10.1016/0273-1177(90)90386-E.

Gerber, E. P. and D. W. J. Thompson (2017). What makes an Annular Mode "Annular"?, J. Atmos. Sci., 74, 317-332, doi:10.1175/JAS-D-16-0191.1.

Held, I. M. and T. Schneider (1993). The Surface Branch of the Zonally Averaged Mass Transport Circulation in the Troposphere, J. Atmos. Sci., 56, 1688-1697, doi:10.1175/1520-0469(1999)056<1688:TSBOTZ>2.0.CO;2.

Hinssen, Y., A. van Delden, T. Opsteegh and W. de Geus (2010). Stratospheric impact on the troposphere deduced from potential vorticity inversion in relation to the Arctic Oscillation, Quart. J. R. Meteorol. Soc., 136, 20-29, doi:10.1002/qj.542.

Hinssen, Y., A. van Delden and J. Opsteegh (2011). Influence of Sudden Stratospheric Warmings on tropospheric winds, Meteorol. Zeitschrift, 20, 259-266, doi:10.1127/0941-2948/2011/0503.

Holton, J. R. (2004). An Introduction to Dynamic Meteorology, Fourth Edition, Elsevier Academic Press, 529, ISBN:0-12-354015-1.

Holton, J. R., P. H. Haynes, M. E. McIntyre, A. R. Douglas et al. (1995). Stratosphere-troposphere exchange, Rev. Geophys., 33, 403-439, doi:10.1029/95RG02097.

Hoskins, B. (1991). Towards a PV-θ view of the general circulation, Tellus, 43AB, 27-35, doi:10.3402/tellusb.v43i4.15396.

Hoskins, B. J., M. E. McIntyre and A. W. Robertson (1985). On the use and significance of isentropic potential vorticity maps, Quart. J. R. Met. Soc., 111, 877-946, doi:10.1002/qj.49711147002.

Hurrell, J. W. (1995). Decadal trends in the North Atlantic Oscillation: regional temperatures and precipitation, Science, 269, 676-679, doi:10.1126/science.269.5224.676.

Iwasaki, T., T. Shoji, Y. Kanno, M. Sawada et al. (2014). Isentropic Analysis of Polar Cold Airmass Streams in the Northern Hemispheric Winter, J. Atmos. Sci., 71, 2230-2243, doi:10.1175/JAS-D-13-058.1.

Johnson, D. R. (1989). The forcing and maintenance of global monsoonal circulations: an isentropic analysis, Adv. Geophys., 31, 43-316, doi:10.1016/S0065-2687(08)60053-9.

Kanno, Y., M. R. Abdillah and T. Iwasaki (2015). Charge and discharge of polar cold air mass in Northern Hemispheric winter, Geophys. Res. Lett., 42, 7187-7193, doi:10.1002/2015GL065626.

Li, J. and J. X. L. Wang (2003). A modified zonal index and its physical sense, Geophys. Res. Lett., 30, 1632, doi:10.1029/2003GL017441.

Li, S., J. Perlwitz, M. P. Hoerling and X. Chen (2010). Opposite Annular Responses of the Northern and Southern Hemispheres to Indian Ocean Warming, J. Clim., 23, 3720-3738, doi:10.1175/2010JCLI3410.1.

Lorenz, E. N. (1951). Seasonal and irregular variations of the northern hemisphere sea-level pressure profile, J. Meteorol., 8, 52-59, doi:10.1175/1520-0469(1951)008<0052:SAIVOT>2.0.CO;2.

Manola, I., F. Selten, H. de Vries and W. Hazeleger (2013). "Waveguidability" of idealized jets, J. Geophys. Res., 118, 10432-10440, doi:10.1002/jgrd.50758.

Nagle, F. W. (1979). Visualizing a Cold Air Dome, B. Am. Meteorol. Soc., 60, 128, doi:10.1175/1520-0477-60.2.128.

Namias, J. (1950). The index cycle and its role in the general circulation, J. Meteorol., 7, 130-139, doi:10.1175/1520-0469(1950)007<0130:TICAIR>2.0.CO;2.

Randall, D. (2015). An Introduction to the Global Circulation of the Atmosphere, Princeton University Press, 442, ISBN:978-0-691-14896-0.

Riviere, G. and M. Drouard (2015). Dynamics of the Northern Annular Mode at Weekly Time Scales, J. Atmos. Sci., 72, 4569-4590, doi:10.1175/JAS-D-15-0069.1.

Rogers, J. C. (1981). The North Pacific Oscillation. International Journal of Climatology, 1, 39-57, doi:10.1002/joc.3370010106.

Rosenlof, K. H. (1995). Seasonal cycle of the residual mean meridional circulation, J. Geophys. Res., 100, D3, 5173-5191, doi:10.1029/94JD03122.

Rowntree, D. (1981). Statistics Without Tears. Penguin updated edition, 2018, 199, ISBN:978-0-141-98749-1.

Schneider, T. (2006) The General Circulation of the Atmosphere, Annu. Rev. Earth Planet. Sci., 34, 655-688, doi:10.1146/annurev.earth.34.031405.125144.

Scott, R. K. and J. P. Cammas (2002). Wave breaking and mixing at the sub-tropical tropopause, J. Atmos. Sci., 59, 2347-2361, doi:10.1175/1520-0469(2002)059<2347:WBAMAT>2.0.CO;2.

Shaw, N. (1931). Manual of Meteorology, 4, Cambridge University Press, London, 328.

Thompson, D. W. J. and J. M. Wallace (1998). The Arctic Oscillation signature in the wintertime geopotential height and temperature fields, Geophys. Res. Lett., 25, 9, 1297-1300, doi:10.1029/98GL00950.

Thompson, D. W. J. and J. M. Wallace (2000). Annular modes in the extra-tropical circulation. Part I: Month-to-Month Variability, J. Clim. 13, 1000-1016, doi:10.1175/1520 0442(2000)013<1000:AMITEC>2.0.CO;2.

Thorpe, A. J. (1993). An appreciation of the meteorological research of Ernst Kleinschmidt, Meteorol. Zeitschrift, 2, 3-12, doi:10.1127/metz/2/1993/3.

Vallis, G. K. and E. P. Gerber (2008). Local and hemispheric dynamics of the North Atlantic Oscillation, annular patterns and the zonal index, Dynam. Atmos. Oceans, 44, 3-4, 184-212, doi:10.1016/j.dynatmoce.2007.04.003.

Wallace, J. M. (2000). North Atlantic Oscillation/Annular Mode: two paradigms, one phenomenon, Q. J. R. Meteor. Soc., 126, 791-805, doi:10.1002/qj.49712656402.

Yu, Y., R. Ren and M. Cai (2015). Comparison of the mass circulation and AO indices as indicators of cold air outbreaks in northern winter, Geophys. Res. Lett., 42, 2442-2448, doi:10.1002/2015GL063676.

***CORRESPONDING AUTHOR: Aarnout J. VAN DELDEN**,
Institute for Marine and Atmospheric Research Utrecht (IMAU), Physics Department, Utrecht University,
Princetonplein 5, 3584CC Utrecht, the Netherlands
e-mail: a.j.vandelden@uu.nl